



## Solvent mixing and ion partitioning effects in spontaneous charging and electrokinetic flow of immiscible liquid-liquid interface

Yunfan Huang  and Moran Wang \**Department of Engineering Mechanics, Tsinghua University, Beijing 100084, China*

(Received 15 June 2024; accepted 5 September 2024; published 9 October 2024)

Electrokinetic transport occurs at the two-liquid interfaces due to its inevitably spontaneous charging induced by imbalanced partition and/or specific adsorption. The diffuse feature of the liquid-liquid interface is essential in interpretation of its electrokinetic behavior and the interplay of the two charging mechanisms is strongly dependent on the interfacial physicochemical properties, which are often ignored in previous studies and may lead to the impractical electrokinetic predictions. We propose a diffuse interface framework which includes a modified Boltzmann formulation, to incorporate the solvent mixing effect and unify the description of both possible charging mechanisms. The permittivity- and viscosity-related solvent mixing effects are stressed when imbalanced ion partition dominates and the viscosity ratio is large. The effects of permittivity-dependent ion partition and organic impurity ions are exhaustively discussed for nonpolar and polar organic liquids. For polar organic liquid with moderate permittivity, the water velocity presents a nonmonotonic dependency on the impurity concentration under different pHs, resulting from the competitive effect of the two charging mechanisms. A semiempirical correction formula for the sharp interface model is proposed to eliminate the modeling deviations, while the viscosity interpolation model is demonstrated to have a great impact on the interpretation of the electroosmotic velocity profile. Our work sheds light on the further studies of the complex electrokinetic multiphase flows with complex geometry, large deformation, contact line dynamics, and weak nonequilibrium transport.

DOI: [10.1103/PhysRevFluids.9.103701](https://doi.org/10.1103/PhysRevFluids.9.103701)

### I. INTRODUCTION

Immiscible fluid-liquid interface plays essential roles in hydrophobic interaction and biological self-assembly [1–3], nerve conduction along nerve fiber and at synapse [4–6], solvent-based extraction and phase-separation-induced active spreading [7–9], wettability alteration and enhanced oil recovery [10–12], and other scenarios, in which the quantitative regulation of its interfacial dynamics of fluid and ion is emphasized. Electrokinetics, stemming from the colloid and interface science in the early days and nowadays extending to the interface electromechanics and physicochemical hydrodynamics, focuses on the flow and motion induced by the ion-fluid coupling interfacial transport within the electrolyte solutions (especially the strong electrolytes) near a prescribed charged interface. In this work, we will focus on the spontaneous charging and electrokinetic flow of the interface between two immiscible electrolyte solutions (ITIES), while the so-called aqueous two-phase solutions (ATPS) due to the solute phase separation within the aqueous solution as well as the interface between liquid metal and aqueous solution with a high interface tension is beyond our scope in this work [13–15].

\*Contact author: [mrwang@tsinghua.edu.cn](mailto:mrwang@tsinghua.edu.cn)

Although there have been plenty of applications on this topic, such as electric pumping and energy harvesting in micro-/nano-channels [16–20], microfluidic droplet manipulation [21–24], and the wettability-alteration-based regulation of multiphase flow in porous media [25], the complex electrokinetic characteristics of two-liquid interface is far from well understood and remains quite challenging to quantitatively capture up to now, which limits the interpretation and prediction of the basic electrokinetic multiphase flows, such as two-liquid parallel electroosmosis and droplet/bubble electrophoresis in the electrokinetic measurement of two-liquid interface charging [26]. In terms of the physicochemical electrokinetic behavior, the two-liquid interface has two fundamentally distinct features compared with the solid-water interface, i.e., the solvent mixing effects and ion partitioning effects.

On the one hand, going through the literature on the electrochemistry of liquid-liquid interface, imbalanced partition (of cations and anions between two bulk phases) and specific adsorption (of interface-active ions from bulk phases to solvent mixing layer, including the dissociation of surface groups and the specific adsorption of polyvalent ions and ionic surfactants) can be recognized as the two major mechanisms of two-liquid interface charging [27–29]. In fact, unlike solid-water and air-water interface which is generally polarizable to most electrolyte ions and the spontaneously interface charged by the specific effective adsorption, the two-liquid interface is acknowledged as partially nonpolarizable (or with a similar physical meaning, partially polarizable), and thus the ion partition effect should be taken into consideration. Basically, the two-liquid partition coefficient roughly denotes the relative activity of a specific ion between the organic liquid and water phases under equal-electrical-potential condition, and is strongly dependent on the solvophobic property of ionic species as well as the permittivity difference between the two solvents [30–33]. For simple metal ions or halide ions in water, the imbalanced partition-induced interface charging at two-liquid interface is negligible since the total amount of net charge in each phase is in trace amount and the organic phase can be considered as dielectrics. However, when there are a few organic ions within the organic phase as inert impurity or active extraction reagents, it will form an interface between two immiscible electrolyte solutions, where the potential drop within the water phase is significant and the imbalanced partition-induced interface charging cannot be ignored [26]. Besides, the solvent mixing layer, which is induced by capillary fluctuation of interface and thermal motion of solvent molecule, will lead to a potential drop strongly dependent on the distribution potential and interface charge density, which may even be comparable to the one across the diffuse layer [34]. However, few previous studies account for those effects in two-liquid electrokinetic flows, and conceptual confusion even exists extensively when reviewing the phenomenological interface potential introduced by some previous literatures [17,35].

On the other hand, when the ionic concentration of aqueous solution is large enough ( $\geq 1$  mM), the thickness of diffuse layer is roughly less than 10 nm, which is almost within the same magnitude as the solvent mixing layer thickness ( $\lesssim 1$  nm) in general, indicating that the interfacial stress induced by the large shear rate within the diffuse layer due to the electrokinetic effect may be strongly impacted by the continuous transition of dynamic viscosity across the solvent mixing layer. Besides, the two electrical diffuse layers will have the same sign and form the electrical triple layer if the interface charging is mainly induced by specific adsorption, while the dominance of imbalanced partition will result in the electrical double diffuse layers with different signs of the net charges. In a variety of two-liquid interfacial electrokinetic systems, the electrokinetic behavior exhibits variation as a result of the distinct charging mechanisms that prevail within each system. Thus, it is indicated that the interpretation of the two-liquid interfacial electrokinetic flow behavior should be heavily dependent on the choice of specific charging mechanism and the interpolation function of the material properties across the interface, which are closely related to the interfacial physicochemical properties of the system. However, the previous studies on the liquid-liquid electrokinetic flow usually focus on single charging mechanism [24,36–38]. There are only a few studies considering both of the two charging mechanisms in their physical models of droplet electrophoresis and two-liquid electroosmosis [35,39,40], while many of them directly use the phenomenological interfacial charge density and distribution potential rather than *a priori*

value specified by the system-dependent constraints. The material properties are also assumed discontinuous instead of a continuous transition around the two-liquid interface in those works, which may result in the wrong interpretation when the viscosity ratio becomes large.

It is thus necessary to incorporate the diffuse feature of the two-liquid interface into the description of the electrokinetic multiphase flow systems to account for the aforementioned two effects. To describe the evolution of flexible liquid-liquid interfaces, there are basically two categories of models, i.e., sharp interface models and diffuse interface models [41–43]. The former is based on a geometric zero-thickness interface, defined under a certain equivalence assumption on the phase partition and leading to apparent surface energy excess called interface tension, while the latter one utilizes a continuous phase distribution as well as the interface stress across the interface, allowing for a unified description of multiphysical transport in the whole domain. As a typical interfacial ion-fluid coupling transport problem, the possible ion partition-adsorption behavior and large gradient of physical fields at a flexible interface are hard to capture in a manner of sharp interface. In fact, the sharp interface model is only able to provide *a posteriori* determination of solvent mixing layer potential jump [17,35]. It will also inevitably lead to significant errors in velocity profiles around the interface due to the inaccuracy of interfacial stress-matching condition, especially as both dynamic viscosity ratio and interfacial shear rate reach large values which arises from the electroosmosis to the opposite direction within the interfacial electrical layers.

On the contrary, the diffuse interface model has the strength to resolve those transitions of material properties and physical fields naturally, and is thus suitable for the accurate modeling of the two-liquid electrokinetic problem [44,45]. However, different from the liquid-liquid multiphase flow without multiphysical transport, the interface thickness determination and material property interpolation in the two-liquid interfacial charging and its electrokinetic flow become a physically essential problem instead of a purely numerical issue, given that the electrokinetic behavior is highly sensitive to the details inside the electrical diffuse layer and the solvent mixing layer both of which are lying within the nanoscales. In this work, we will emphasize the diffuse feature of interfacial charging and electrokinetic flow of the two-liquid multiphase systems with the diffuse interface models.

The challenge of modeling the interphase transport behaviors of both liquid phases and charged species lies in the inevitable deformation and motion of liquid-liquid interface. As the flexible interface may experience a large deformation or long-distance motion which is commonly met in droplet electrophoresis and wetting dynamics, the part of domain that requires a high resolution is not fixed and only confined within the initial interface region but may sweep over a large space as the interface evolves. Besides, there are also various possibilities of interphase charge dynamics according to the specific interfacial polarizability and strength of nonequilibrium potential, and we will limit our scope within the near-equilibrium case where the interface charge distribution retains its initial equilibrium as the interface evolves, while interphase charge relaxation and kinetic transport leading to the ion redistribution will be ignored [46–49].

Another challenge is to capture the complex interaction between ions and solvent molecules along with the interface deformation and motion, on which several researchers utilize the free energy or pseudopotential methods but are only able to mimic the ion partition effect [50–53]. Though the equilibrium distribution of ion concentration was verified in those works, a quantitative evaluation for liquid-liquid interfacial electrokinetic models is still lacking. In addition, the absence of adsorption mechanism in these models is mainly due to the high computational cost originating from the required high interface resolution to include the charge adsorption layer whose thickness is about 1 nm and much smaller than the diffuse layer thickness, while those numerical methods (such as the lattice Boltzmann method) are based on the regular and uniform grid and it is rather complicated to deal with such issues using the multiblock techniques. Therefore, a proper treatment of coupling behavior of charges and solvents at interface to embed the general charging mechanisms and electrokinetic flow into a diffuse and flexible interface model is required.

In this article, we aim to address the permittivity- and viscosity-related solvent mixing effects and permittivity- and component-dependent ion partitioning effects in electrokinetic multiphase

flow and choose the two-liquid parallel electroosmosis as the model system to illustrate the underneath physics. Essentially, the dependence of ion partition coefficient on permittivity and charged species will be first relaxed and set as free parameters, and then the constraints will be taken into consideration. A unified description of ion partition- and adsorption-induced spontaneous interface charging is proposed for the first time in a formulation of modified Boltzmann distribution and effective additional Gibbs free energy profile, and then coupled with the electrokinetic multiphase flow at diffuse interfaces. The proposed framework paves the way to incorporate the electrokinetic effects into more complex multiphase flow systems.

The article is organized as follows. In Sec. II, a brief overview on typical charging mechanisms of two-liquid interface is given, after which the physical model, problem setup and the numerical method are given. In Sec. III, the solvent mixing effects are discussed based on the benchmark studies with single charging mechanism. Then effects of solvent permittivity and organic impurity ions on the interfacial charging behavior are studied for the realistic two-liquid systems with simple ions, in which the interplay of the two charging mechanisms is stressed. Conclusions and perspectives are summarized in Sec. IV.

## II. MODELS AND METHODS

### A. Phase evolution: Cahn-Hilliard-Navier-Stokes equations

To obtain the detailed ionic distribution structure of the two-liquid interface, we will first introduce the description of the diffuse interface deformation and evolution in this subsection, and then elucidate the ionic distribution structure within and around the interface in the following parts. As elucidated before, it is difficult to get reasonable results for the two-liquid electrokinetic problem based on the sharp interface models, which, in addition, is hard to deal with the motion of flexible interfaces with large deformation and topological evolution even if the moving meshing technique is used. It is thus necessary to develop a diffuse-interface-based electrokinetic model to accurately capture the flexible interfacial dynamics with multiphysical transport, as will be introduced below.

Apart from mercury-solution interface with a high interface tension, the two solvent phases of the immiscible two-liquid interface generally present a diffuse feature into each other rather than maintaining a geometrically flat interface. The phase order parameter  $\phi$  is usually used to describe the phase partition within a small control volume. For an two-liquid two-component system,  $\phi$  have values of  $-1$  and  $1$  within the bulk region of water and organic liquid phases, respectively, and varies continuously across the interface, which is also related to the volume fraction  $\phi_\alpha$  of each phase  $\alpha$  ( $=w, o$ ). The detailed equilibrium profiles near a flat interface are written as

$$\begin{aligned} \phi(\mathbf{x}) &\equiv \tilde{\phi}(D_{\text{int}}) = \tanh\left(\frac{D_{\text{int}}(\mathbf{x})}{d_{\text{pf}}}\right), \\ \phi_o &= \frac{1 + \phi}{2}, \quad \phi_w \equiv 1 - \phi_o = \frac{1 - \phi}{2}, \end{aligned} \tag{1}$$

where  $D_{\text{int}} \equiv D_{\text{int}}(\mathbf{x})$  denotes the signed distance from point  $\mathbf{x}$  to the interface, and  $d_{\text{pf}}$  is the characteristic thickness of the solvent mixing layer. From the nonequilibrium thermodynamics theory and molecular dynamics simulation, when temperature is far from the critical temperature of the solvents, the typical value of  $d_{\text{pf}}$  for an immiscible two-liquid interface is around  $0.1\text{--}1$  nm [54].

The evolution of phase order parameter obeys the Cahn-Hilliard equation

$$\frac{\partial \phi}{\partial t} + \mathbf{u} \cdot \nabla \phi = \nabla \cdot (M \nabla \mu_\phi), \tag{2}$$

where  $\mathbf{u}$  is the local fluid velocity,  $M = \chi(\phi)\varepsilon_{\text{pf}}^2$  is the mobility parameter which determines the characteristic time scale of phase separation, and  $\mu_\phi = \Lambda[-\nabla^2 \phi + (\phi^2 - 1)\phi/\varepsilon_{\text{pf}}^2]$  is the chemical

potential deduced from the following Landau free energy [55]

$$\Psi = \int \left[ c_s^2 \bar{\rho} \ln \bar{\rho} + \frac{\Lambda}{2} \left( (\nabla \phi)^2 + \frac{(\phi^2 - 1)^2}{2\varepsilon_{\text{pf}}^2} \right) \right] dV, \quad (3)$$

where the first term in the bracket is the ideal solution bulk free energy with phase interpolated density  $\bar{\rho}$  and sound velocity  $c_s$ , and the second and third term determines the phase separation behavior and gives the interface energy excess due to the local inhomogeneity of the phase distribution. We can obtain the interface tension coefficient from the integration across a flat interface

$$\gamma = \int_{-\infty}^{\infty} \left[ \frac{\Lambda}{2} \left( (\nabla \phi)^2 + \frac{(\phi^2 - 1)^2}{2\varepsilon_{\text{pf}}^2} \right) \right] dn = \frac{2\sqrt{2}}{3} \frac{\Lambda}{\varepsilon_{\text{pf}}}, \quad (4)$$

which indicates the interface is immiscible only when the condition  $\Lambda > 0$  is met. Setting  $\mu_\phi = 0$ , the equilibrium phase profile is derived in the same form as Eq. (1) which gives  $d_{\text{pf}} = \sqrt{2}\varepsilon_{\text{pf}}$ . It is seen that once the interface tension  $\gamma$  and interface thickness parameter  $\varepsilon_{\text{pf}}$  are prescribed, the phase separation parameter  $\Lambda$  is then determined. The no flux condition for  $\mu_\phi$  at solid wall is utilized [56], i.e.,  $\nabla_n \mu_\phi = 0$ , and the contact angle  $\theta$  is imposed in a geometric manner [25], i.e.,  $\nabla_n \phi = |\nabla \phi| \cos \theta$ .

The Navier-Stokes equations are utilized for the incompressible fluid flow

$$\begin{aligned} \nabla \cdot \mathbf{u} &= 0, \\ \bar{\rho} \frac{\partial \mathbf{u}}{\partial t} + \bar{\rho} \mathbf{u} \cdot \nabla \mathbf{u} &= -\nabla p + \nabla \cdot (\bar{\mu} \nabla \mathbf{u}) + \mathbf{F}_{\text{st}} + \mathbf{F}_e. \end{aligned} \quad (5)$$

Here,  $\mathbf{u}$ ,  $p$  are the fluid velocity and pressure, respectively.  $\mathbf{F}_{\text{st}} \equiv -\phi \nabla \mu_\phi$  is the original form of interface tension, which can be transformed into  $\mathbf{F}_{\text{st}} = \mu_\phi \nabla \phi$  in our treatment and then requires only a second-order derivative of  $\phi$  in numerical discretization while the potential gradient term  $-\nabla(\mu_\phi \phi)$  has been absorbed into the pressure term.  $\mathbf{F}_e = \rho_e \mathbf{E} - (1/2)E^2 \nabla \bar{\varepsilon}$  is the electromechanical force derived from the Maxwell stress, where  $\rho_e$  is the local volume charge density in solution and we have incorporated the electrostriction term which is also a potential gradient term into the pressure term. Here,  $\mathbf{E} = -\nabla \varphi$  is the overall electric field, which includes the internal field induced by the interfacial physicochemical effects (see Sec. II B) and the external field triggered by the external voltage source (see Sec. II C). Concerning the material properties,  $\bar{\rho}$ ,  $\bar{\mu}$ , and  $\bar{\varepsilon}$  are the local phase interpolations of fluid density, dynamic viscosity, and permittivity, respectively, whose specific formulations will be given in Sec. II C. No-slip boundaries are utilized for fluid flow, noting that with the above boundary condition of phase order parameter, a moving contact line can still be regularized through the phase diffusion [56].

### B. Equilibrium potential distribution: Modified Poisson-Boltzmann formulation

To include the specific charging mechanism and charge distribution profile, plenty of interface charging models have been proposed, among which the generalized electrical layer model and modified free energy profile model have great performance to balance the effectiveness and efficiency, and also relatively well validated with the electrochemical and electrocapillary experiments [29]. To accommodate with the diffuse feature of the two-liquid interface as well as its flexible characteristics, it is preferable to use the modified free energy profile to provide a unified description of both partition and adsorption effects and to capture the possible dynamic behaviors of ions within and around the solvent mixing layers [57,58]. Besides, since the two-liquid interface with a ‘‘fluid-mosaic’’-like structure provides no fixed adsorption site, the utilization of quasi-thermodynamic adsorption isotherm based on the modified free energy formulation is also more favorable for the description of its specific charging mechanism than the surface complexation models which are based on the chemical kinetics and widely used in solid-solution interface [22].

The equilibrium distribution of charged species can be described by the following modified Boltzmann distribution

$$n_i = n_{i,w} \exp \left[ -\frac{z_i e \varphi}{k_B T} - \frac{\Delta g_i(\phi)}{k_B T} \right], \quad (6)$$

followed by the Poisson equation for the electric potential  $\varphi$ ,

$$\nabla \cdot (\bar{\epsilon} \nabla \varphi) = -\rho_e + \rho_{\text{fix}}. \quad (7)$$

Considering the equilibrium distribution of ions at two-liquid interface, the total additional Gibbs free energy profile  $\Delta g_i(\phi) \equiv \Delta_w g_i(\phi) := \mu_i(\phi) - \mu_i(-1)$  capturing the partition-adsorption behavior of solute ions is assumed to be only related to the phase order parameter  $\phi$ ;  $n_i$  is the number density of ion  $i$ ,  $n_{i,w} \equiv n_{i,\infty}^{(w)}$  is  $n_i$  within the bulk and electrically neutral region in the water phase. The volume charge density of ions is expressed in  $\rho_e = \sum_i z_i e n_i$ , and  $\rho_{\text{fix}}$  is the fixed charge density which may be included when there is specific adsorption at interface, as will be introduced later. It is noteworthy that the above formulation is called the *modified* Poisson-Boltzmann equation because the free energy is a single-particle description in a manner of mean force field which could effectively incorporate the correlation effect between double diffuse layers, ion penetration and steric effects around solvent mixing layer, and image effects through solvent mixing layer with nonuniform permittivity. It is indicated that the detailed form of the real free energy profile  $\Delta g_i(\phi)$  should be upscaled from the particle statistics of ionic structure, especially for cases of strong ion correlation or near-saturated adsorption, which is beyond our scope of this work.

To determine the charge distribution, the details of the Gibbs free energy profile  $\Delta g_i(\phi)$  in the continuous models for the electrokinetic flow should be given, which is related to the overall Gibbs free energy of transfer and adsorption. For the details of two-liquid interfacial charging mechanism, see Appendix A. As a primary study, here we will use the step potential models for this extension [59]. According to the specific charging mechanism of the interface, we classify the possible situations into three cases: (1) pure specific adsorption, (2) pure imbalanced partition, and (3) mixed charging mechanism with both. The total additional free energy profile  $\Delta g_i(\phi)$  of ion  $i$  is then decomposed into two parts,

$$\Delta g_i(\phi) = \Delta g_i^{(t)}(\phi) + \Delta g_i^{(a)}(\phi), \quad (8)$$

whose energy profile can be phenomenologically decomposed to two parts, i.e., partition-induced one

$$\Delta g_i^{(t)}(\phi) = \begin{cases} 0, & \phi \leq \tilde{\phi}(d_{\text{part}}), \\ \Delta g_{t,i}, & \phi > \tilde{\phi}(d_{\text{part}}), \end{cases} \quad (9)$$

and (specific) adsorption-induced one

$$\Delta g_i^{(a)}(\phi) = \begin{cases} 0, & \phi \leq \tilde{\phi}(d'_{\text{ad}}) \text{ or } \phi \geq \tilde{\phi}(d_{\text{ad}}), \\ \Delta g_{a,i}, & \tilde{\phi}(d'_{\text{ad}}) < \phi < \tilde{\phi}(d_{\text{ad}}). \end{cases} \quad (10)$$

For convenience, the simplified symbols of free energy are defined as  $\Delta g_{t,i} \equiv \Delta_w^0 g_{t,i}^0$  and  $\Delta g_{a,i} \equiv \Delta_w^i g_{a,i}^0$ . Note that the discontinuity of  $\phi$  at  $\mathbf{x}$  can be smoothed out using a smoothing operator  $\mathcal{S}_n(\mathbf{x}, \alpha_S)$  with a total thickness of  $d_S = |\tilde{\phi}^{-1}(D_{\text{int}}(\mathbf{x}) + \alpha_S/2) - \tilde{\phi}^{-1}(D_{\text{int}}(\mathbf{x}) - \alpha_S/2)| \simeq \alpha_S/|\tilde{\phi}'(D_{\text{int}}(\mathbf{x}))|$  and the continuity to the  $n$ -th derivatives over  $\tilde{\phi}$ . As default, for cases (1) and (3), we fix  $d_{\text{ad}} = -d'_{\text{ad}} = d_{\text{pf}}$  with  $\mathcal{S}_2(\pm d_{\text{pf}}, 0.01)$ , while we set  $d_{\text{part}} = 0$  and  $d_{\text{part}} = -d'_{\text{ad}} \equiv -d_{\text{pf}}$  for cases (2) and (3) with  $\mathcal{S}_2(0, 1)$  and  $\mathcal{S}_2(-d_{\text{pf}}, 0.01)$ , respectively.

To define the interface charging parameters including the additional Gibbs free energies  $\Delta g_{\text{alt},i}$ , the distribution potential  $\Delta_w^0 \varphi_\infty$ , the ion concentration ratio (distribution ratio)  $n_r$ , and the fixed charge density  $\rho_{\text{fix}}$ , two series of approaches are provided in this study. One is used for phenomenological parametric study where the prescribed parameters are independently tuned, the other

is derived from specific charging mechanism of the specific two-liquid interface system where there are interfacial physicochemical constraints on the feasible region of parameters. The former approach [called approach (A)] will be utilized for the verification and validation of our proposed numerical method and physicochemical models, including the discussions on the permittivity-dependent and viscosity-dependent solvent mixing effect, referred to Secs. III A 1 and III A 2, respectively. The latter approach [called approach (B)] will be used in the study of organic impurity and permittivity effects on the interface charging and electrokinetic flow behavior of different two-liquid interface systems (see Sec. III B). To elucidate the details of the two approaches and simplify the formulation, we nondimensionalize the equilibrium distribution potential  $\Delta_w^0 \varphi_\infty$ , solvent mixing layer potential drop  $\Delta\varphi_i$ , and free energy barriers/wells  $\Delta g_{a,i}$  and  $\Delta g_{t,i}$  using characteristic values of  $\zeta_T \equiv k_B T/e$  and  $k_B T$ , denoted by  $\Phi_\infty$ ,  $\Phi_i$  and  $\mathcal{G}_{a|t,i}$ , respectively.

In approach (A), the required free energy of transfer  $\mathcal{G}_{t,\pm}$  for prescribed equilibrium distribution potential  $\Phi_\infty$  and ion partition ratio  $n_r \equiv n_{\pm,o}/n_{\pm,w}$  can be derived as follows from Eqs. (A2) and (A3):

$$-\frac{\mathcal{G}_{t,+} + \mathcal{G}_{t,-}}{2} = \ln n_r, \quad -\frac{\mathcal{G}_{t,+} - \mathcal{G}_{t,-}}{2} = \Phi_\infty. \quad (11)$$

Again we only give the results of 1:1 electrolytes here for illustration. As for the free energy of adsorption, it is straightforward to define the effective volume charge density  $\rho_{\text{fix}}$  of the interface specifically adsorbed ion with the prescribed surface charge density  $\sigma_{\parallel}$

$$\rho_{\text{fix}}(\phi) = \begin{cases} \sigma_{\parallel}/2d_{\text{pf}}, & |\phi| \leq \tilde{\phi}(d_{\text{pf}}), \\ 0, & |\phi| > \tilde{\phi}(d_{\text{pf}}), \end{cases} \quad (12)$$

with  $\mathcal{G}_{a,i} \gg 1$  leading to  $\rho_e \rightarrow 0$  at interface, where  $\sigma_{\parallel}$  is set to constant here. Here we relaxes the constraints between distribution potential (as well as the ionic concentration ratio) and permittivity ratio and ignores the possible adsorption isotherms to determine the interface charge density according to the bulk ionic concentration.

In approach (B), the free energies of transfer for certain charged interface system could be given by either Born potential model or nonlocal electrostatics method, which should be validated by experimental results. As for the interface adsorbed charge density, it is rather easy to make use of Eq. (12) where  $\sigma_{\parallel}$  can be derived from the required complex mechanism in equilibrium adsorption, while here we choose another more natural way to incorporate the specific adsorption using free energy formulation which can be further extended to describe the nonuniform interface charging in weak nonequilibrium cases induced by charge convection. Defining  $\zeta_{\parallel}^{(w)} = \varphi(\mathbf{x})|_{D_{\text{int}}(\mathbf{x})=-d_{\text{pf}}}^{D_{\text{int}}(\mathbf{x})<-\lambda_{\text{D,w}}}$  as the  $\zeta$  potential on the water side, it is obtained that

$$\sigma_{\parallel} \simeq z_{i_0} e \times 2d_{\text{pf}} K_{a,i_0} n_{i_0,w} \exp\left(-\frac{z_{i_0} e \zeta_{\parallel}^{(w)}}{k_B T}\right) \equiv 2d_{\text{pf}} K_{a,i_0} \rho_{\parallel}, \quad (13)$$

with  $\mathcal{G}_{a,i_0} \sim 1$ ,  $\mathcal{G}_{a,\bar{i}_0} \gg 1$ , and  $\rho_{\text{fix}} = 0$ . Here,  $i_0$  is the adsorbed ion at interface while  $\bar{i}_0$ s represent the other ions assumed to be depleted at interface, and  $K_{a,i_0} = \exp(-\mathcal{G}_{a,i_0})$  is the specific adsorption coefficient of ion  $i_0$ . It is obvious that the interface charge density  $\sigma_{\parallel}$  is linear to the local volume charge density  $\rho_{\parallel}$  of free ions at the plane where  $\zeta_{\parallel}^{(w)}$  is defined, which implies a linear adsorption isotherm for a prescribed free energy of adsorption  $\mathcal{G}_{a,i_0}$ . Note that since  $|\Delta\varphi_i| \ll |\zeta_{\parallel}^{(w)}|$  is not always satisfied for an two-liquid interface, the above evaluation of interface charge has a normalized deviation about  $\exp(\pm\Phi_i)$  where the solvent mixing layer potential drop may play an essential role.

For the boundary condition at solid wall  $\Gamma_{\text{ls}}^{(\alpha)}$  in contact with liquid phase  $\alpha$ , the constant  $\zeta$  potential condition is written as

$$(\varphi - \varphi_\infty^{(\alpha)})|_{y \in \Gamma_{\text{ls}}^{(\alpha)}} = \zeta_{\text{ls}}^{(\alpha)}, \quad (14)$$

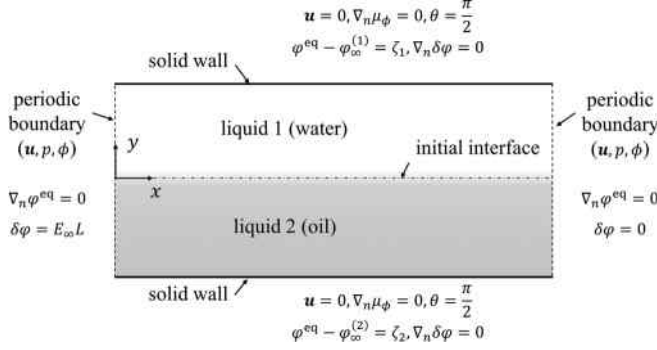


FIG. 1. Schematics of the two-liquid parallel electroosmosis system setup.

and the constant surface charge density condition is written as

$$\mathbf{n} \cdot \varepsilon_\alpha \nabla \varphi|_{y \in \Gamma_{\text{ls}}^{(\alpha)}} = -\sigma_{\text{ls}}^{(\alpha)}, \quad (15)$$

where  $\mathbf{n}$  is the normal vector at the solid wall pointing into the solution. Note that here we have neglected the electrical polarization inside the solid region.

### C. Problem setup and numerical method

In this work, we will focus on the two-liquid parallel electroosmosis in an infinite channel where the internal electric field induced by the interface charging is orthogonal to the external electric field, which incidentally avoids the difficulty in dealing with the coupling between internal and external electric field. Therefore, Eqs. (2), (5), and (6) have constituted a complete set of governing equations for such two-liquid interfacial electrokinetic systems. This is consistent with our assumption that the charge distribution around the two-liquid interface is always in electrochemical equilibrium and maintains its initial relative configuration to the interface, which is reflected by the fact that Eq. (6) can be derived by setting the transient term and convective term in the Nernst-Planck equation (B4) to zero.

The schematics of the two-liquid parallel electroosmosis system to be studied in this work is shown in Fig 1, which is commonly used in the electric pumping of nonconducting or poorly conductive liquid in the microfluidic devices. The liquid phase  $\alpha$  initially occupies a thickness of  $d_\alpha$  in the straight channel with the total width of  $d_{\text{tot}} \gtrsim 1 \mu\text{m}$ , in which  $d_w > 0.5 \mu\text{m}$  is assumed. The ionic strength satisfies  $I_w = \sum_i z_i^2 n_{i,w} / 2 \lesssim 1 \text{mM}$ , which gives a Debye length  $\lambda_{D,w} = [e^2 \sum_i z_i^2 n_{i,w} / (\varepsilon_w k_B T)]^{-1/2} \ll d_w$  indicating that the two electrical diffuse layers at the solid boundaries and the two-liquid interface do not overlap with each other inside the aqueous solution. At the solid walls, the no-slip boundary for velocity and zero normal gradient conditions for chemical potential are utilized and the contact angles are fixed at  $\pi/2$ . Periodic flow and electric potential conditions for  $\mathbf{u}$ ,  $p$ ,  $\phi$  are applied at the inlet and outlet boundaries, i.e.,

$$\mathbf{u}_{\text{in}} = \mathbf{u}_{\text{out}}, \quad p_{\text{in}} - p_{\text{out}} = \Delta p, \quad \phi_{\text{in}} = \phi_{\text{out}}. \quad (16)$$

Here,  $\Delta p$  is set to zero as default. A constant contact angle is applied for the possible contact line, along with a constant interface tension coefficient  $\gamma = 0.05 \text{N/m}$  as a typical value between aqueous solutions and liquid  $n$ -alkanes. As for the electric potential  $\varphi$ , the application of its boundary conditions is divided into the equilibrium distribution  $\varphi^{\text{eq}}$  and its linear perturbation  $\delta\varphi$  whose physical rationale and governing equations are elaborated in Appendix B. For the former, the prescribed  $\zeta$  potentials at the solid boundaries and zero surface charge density at the inlet and outlet boundaries are imposed; while for the latter, the prescribed electric potential at inlet and outlet and

zero surface charge density at the solid boundaries are used. Here,  $E_\infty$  denotes the external electric field and  $L$  denotes the domain width chosen from the straight channel with an infinite length.

In this work, the interface thickness parameter  $\varepsilon_{\text{pf}}$  takes the value of 0.5 nm as a physically reasonable value. The material properties  $\bar{\varepsilon}$ ,  $\bar{\rho}$ ,  $\bar{\mu}$  are assumed to have the following dependence on the volume fraction  $\phi_\alpha$  of phase  $\alpha$  as default ( $\alpha = \text{w}, \text{o}$ )

$$\begin{aligned}\bar{\varepsilon} &\equiv \varepsilon(\phi) = \sum_{\alpha} \varepsilon_{\alpha} \phi_{\alpha}, \\ \bar{\rho} &\equiv \rho(\phi) = \sum_{\alpha} \rho_{\alpha} \phi_{\alpha}, \\ \bar{\mu} &\equiv \mu(\phi) = \sum_{\alpha} \mu_{\alpha} \phi_{\alpha}.\end{aligned}\tag{17}$$

It has been shown that such a linear interpolation strategy for  $\varepsilon(\phi)$  shows no difference from gradient theory or harmonic interpolation function [60,61], while the linear interpolation functions for  $\rho$ ,  $\mu$  are chosen as default following the previous studies [62,63]. Note that the  $\rho(\phi)$  model has little influence on the electrokinetic flow behavior because the transient and inertial effects are negligible in this work. However, when the dynamic viscosity ratio  $\mu_r = \mu_{\text{o}}/\mu_{\text{w}}$  is large, the choice of  $\mu(\phi)$  model may cause derivations of the velocity profiles within the diffuse layer and other viscosity interpolation models may be required, as will be discussed in Sec. III A 2. The phase mobility  $\chi(\phi) \equiv \chi_0 = 10 \text{ m s/kg}$  gives a characteristic timescale of order parameter diffusion  $T_\chi \sim (8\sqrt{2}/3)\varepsilon_{\text{pf}}/\gamma\chi_0 \sim 2.7 \times 10^{-9} \text{ s}$ , which ensures its sufficient relaxation compared with the other processes such as ion diffusion with scaling of  $T_D = \lambda_{\text{D},\alpha}^2/D_{i,\alpha} \sim 1 \times 10^{-8} \text{ s}$  and fluid flow with scaling of  $T_v = d_{\text{tot}}^2/\nu_\alpha \sim 1 \times 10^{-6} \text{ s}$ . Besides, the temperature dependence of the material properties is neglected since the Joule heating is weak for dilute electrolytes and low field strength which is satisfied in this work.

The finite-element method is used to solve the above problem. For the spatial discretization, elements of the second order are used for phase field  $\phi$  and electric potentials  $\varphi^{\text{eq}}$ ,  $\delta\varphi$ , while the first-order and second-order elements are used for the velocity and pressure fields  $\mathbf{u}$ ,  $p$ , respectively. A manually selective meshing refinement is utilized around the charged surfaces and interfaces in the initial configuration to fully resolve the smallest physical scale in this multi-physical transport problem to capture the complete physics correctly while keep the computational cost within an acceptable level. The maximum size of the elements at the two-liquid interface is kept at  $\Delta_{\text{max}}^{\text{surf}} = 0.1\varepsilon_{\text{pf}}$  which ensures the resolution within solvent mixing layer, while the maximum size of bulk elements are set to  $\Delta_{\text{max}}^{\text{bulk}} = 2.5 \text{ nm} < \lambda_{\text{D},\text{w}}$  which along with the transition region from the two-liquid interface is enough to resolve the electric potential within the diffuse layers. The relative error tolerance of the solution is defined as  $10^{-5}$  to ensure the convergence. The element-independence and mesh-independence tests have been conducted which ensures the accuracy of the solution and suppress the spurious force and velocity due to the anisotropy of grid discretization, which ensures the phase interface to retain its initial shape during the two-liquid parallel electroosmosis process without additional external perturbations. To achieve a better stability, an initialization step of phase field is performed according to the initial configuration of phases, and the evolution to the initial distribution of phase field and electric potentials is then calculated, after which a fully coupling solver for steady problems (of electric potentials) or a segregated solver for transient problems (of phase-field evolution and fluid flow) are used to obtain the final steady solution. Since the two-liquid interface may experience a large deformation or move a considerable distance as the system evolves, the adaptive meshing refinement and triangular meshes are used to balance the computational accuracy and stability to achieve a better performance. Note that many of the theoretical and numerical studies make various simplifications and fix the liquid-liquid interface position to avoid the description of complex phase evolution behavior, limiting their applicability within the linear systems with low capillary number and under small external field [47,64–66].

### III. RESULTS AND DISCUSSIONS

#### A. Characteristics of diffuse interface: Solvent mixing effect

A series of benchmark studies following approach (A) are conducted to verify the aforementioned numerical method and to validate the proposed physical model based on a diffuse two-liquid interface, where the distribution potential (or equivalently, the ionic concentration ratio) and interface charge density are treated as free parameters for a parametric study or the quantitative fitting. In particular, the permittivity-related and viscosity-related solvent mixing effects will be addressed in the verification and validation parts, respectively.

##### 1. Permittivity-related effect: Comparison with sharp interface model

Herein, the simulation results from the diffuse interface model are compared with the theoretical solutions to the sharp interface model to verify our numerical methods and to show the permittivity-related solvent mixing effect. For the details of the sharp interface model and its solution, see Appendix C. Without loss of generality, the system dimensions  $d_{\text{tot}} = 1 \mu\text{m}$  and  $d_1 = d_2 \equiv d = d_{\text{tot}}/2$  are assumed in the comparisons. The material properties of the water phase take the values in Appendix D, and the ionic concentration  $c_w \equiv n_w/N_A = 1 \text{ mM}$  of a 1:1 electrolyte solution are fixed (where  $N_A$  is the Avogadro's constant). The material property ratios and ionic concentration ratio between organic liquid and water, i.e.,

$$\varepsilon_r = \frac{\varepsilon_o}{\varepsilon_w}, \quad \mu_r = \frac{\mu_o}{\mu_w}, \quad \rho_r = \frac{\rho_o}{\rho_w}, \quad n_r = \frac{n_o}{n_w}, \quad (18)$$

are tuned by changing material properties and ionic concentration of the organic liquid phase which is generally the case in practice. Here,  $D_{i,\alpha} \equiv D_0 = 5 \times 10^{-9} \text{ m}^2/\text{s}$  is chosen as the typical molecular diffusivity to calculate the solution conductivity  $\bar{\sigma}_c$  when necessary. The electric potentials at solid boundaries are set to  $\zeta_1 = \zeta_2 = \zeta_T$  and all the material property ratios  $\varepsilon_r$ ,  $\mu_r$ ,  $\rho_r$  as well as the bulk ionic concentration ratio  $n_r$  take the value of 1, if no extra explanations are given. Herein, the impact of permittivity ratio on the two-liquid interface charging and electrokinetic flow behavior will be discussed, as shown Fig. 2, while the primary verification results for simplified cases are given in Appendix E.

It is seen that the solvent mixing effect is significant when imbalanced partition dominates the interface charging under large permittivity ratio, as shown in Figs. 2(c) and 2(e). For the partition-induced interface charging, the relative error of the velocity profile is even as large as 20% of the velocity jump across the two-liquid interface when  $\varepsilon_r \equiv \varepsilon_o/\varepsilon_w < 1/20$ . Generally speaking, the theoretical solution of the sharp interface model tends to underestimate the relative velocity between the organic liquid and water phases as well as the shear stress at the two-liquid interface when the imbalanced partition-induced interface charging dominates, while the trend is reversed when the specific adsorption-induced interface charging prevails. This originates from the absence of solvent mixing effect which artificially divides the interfacial region with a continuous transition of material properties into two individual parts with discontinuous material properties separated by the so-called *Gibbs plane*, especially the permittivity [67]. The contrast between the potential gradients at the two-liquid interface from the two sides will be thus attenuated, which reduces the overall potential jump across the interface and results in the inaccuracy of the predictions by sharp interface model. Considering the wide range of possible values of interface charge density, the above errors in the sharp interface model are hard to correct simply through a ‘‘repartition’’ process using a displaced Gibbs plane because of the case-by-case variation of the required artificial displacement.

To account for the above explanations of the deviation in the results, a semiempirical correction formula is proposed then to incorporate the potential drop within the solvent mixing layer into the sharp interface model. First, the local potential gradient normal to the two-liquid interface and

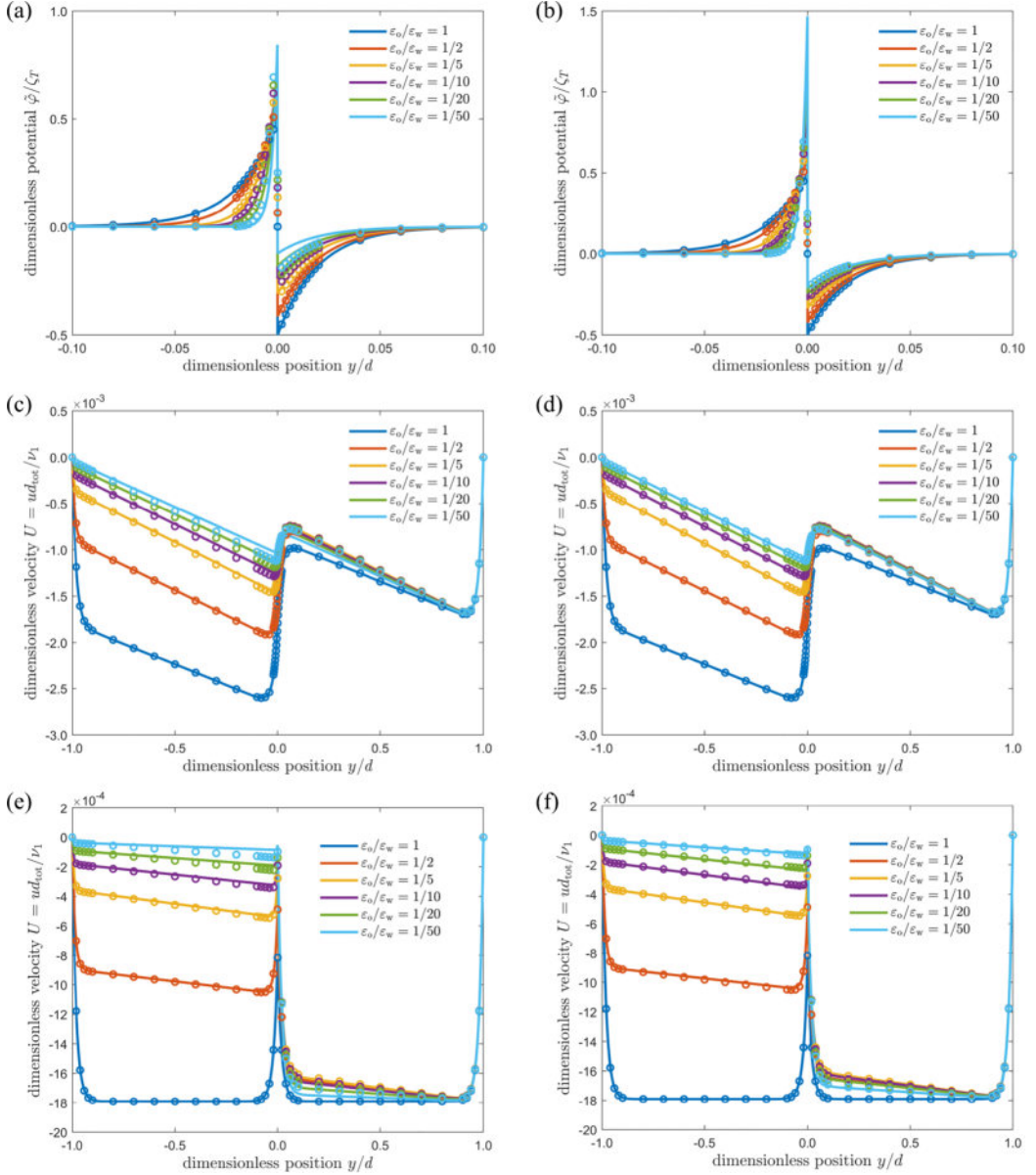


FIG. 2. Dimensionless displaced electric potential and velocity profiles before and after corrections for solvent mixing layer potential drop induced by solvent mixing. The *circles* are the simulation results of the *diffuse interface model*, and the *lines* are the theoretical solutions of the *sharp interface model*. As default, the material property ratios  $\epsilon_r$ ,  $\mu_r$ ,  $\rho_r$  and the bulk ionic concentration ratio  $n_r$  are taken as 1, and  $\zeta_1 = \zeta_2 = \zeta_T$ . Panels (a)–(d) correspond to the pure partition-induced charging with  $\Delta\phi_\infty = -\zeta_T$ , and panels (e) and (f) are the results of pure adsorption-induced charging with  $\sigma_{\text{II}}^w = 0.002 \text{ C/m}^2$ . In particular, the theoretical results (denoted by the circles) in panels (a), (c), and (e) are obtained by setting  $\Delta\phi_{\text{in}} = 0$ , while in panels (b), (d), and (f) the value of  $\Delta\phi_{\text{in}}$  is set to  $\delta\Delta\phi_{\text{in}}$  according to Eq. (20). It is clearly seen that the theoretical results are in great agreement with the diffuse-interface simulation after the solvent mixing layer potential drop correction.

pointing into the phase  $\alpha$  is calculated based on the trial solution with  $\Delta\varphi_i = 0$  mV as follows:

$$\partial_y \varphi_{\alpha,0} = (-1)^{\alpha+1} \frac{\zeta_T}{\lambda_{D,\alpha}} \frac{Z_\alpha - f_\alpha}{\sinh H_\alpha}. \quad (19)$$

Then, the modification of solvent mixing layer potential drop is estimated using

$$\delta\Delta\varphi_i = (\alpha_{\varepsilon,+} \partial_y \varphi_{w,0} + \alpha_{\varepsilon,-} \partial_y \varphi_{o,0}) \frac{\varepsilon_w - \varepsilon_o}{\varepsilon_w + \varepsilon_o} \left( 1 - \frac{4|\sigma_{II}|d_{pf}}{\varepsilon_i \zeta_T} \right), \quad (20)$$

where  $\varepsilon_i = (\varepsilon_w + \varepsilon_o)/2$  is the average permittivity, while  $\alpha_{\varepsilon,\pm} = (\varepsilon_i \pm \varepsilon_o)/(\varepsilon_w + \varepsilon_o)$  fit the contributions from the two sides. The above correction formula is proved to be effective even for large partition coefficient through tests with extreme values of parameters (to  $n_r \simeq 1/1000$ ), which indicates the versatility of the proposed correction formula as well as the essential role of solvent mixing effect. Eq. (20) is expected to be applicable for corrections in more complex scenarios of the two-liquid interfacial electrokinetic flow systems.

## 2. Viscosity-related effect: Comparison with fluid-liquid electrokinetic experiments

The plane-interface technique was invented in 1970s to measure the interface charging parameters of the air-water interface [68], where an open cell is filled with the aqueous solution whose upper boundary coincides with the air-water interface. The voltage is first applied by a pair of electrodes within to drive the electroosmotic flow induced by the solid-water and air-water interface charging, and the PIV technique is utilized using tracer latex particles to visualize the velocity profile. In previous studies, both ionic surfactants and simple ions have been used as solute ions, and a single phase electrokinetic model has been applied with the no-slip boundary assumed at the air-water interface due to the surfactants preventing the interface from moving, which is called the *solidification effect*. Though this is an air-liquid problem, it provides a perfect example where the material property varies sharply across a thin layer (i.e., an effectively solidified surfactant layer) which may dramatically impact the prediction for its electrokinetic behavior. In this study, we will use the typical result with ionic surfactants to validate our physical diffuse interface model and to illustrate the viscosity-related solvent mixing effect by comparing different viscosity interpolation models.

To be specific, the depth of the open cell  $H$  takes the values from 1 mm to 3 mm,  $c_{SDS} = 1 \times 10^{-4}$  M, pH = 5.5,  $c_{NaCl} = 1 \times 10^{-3}$  M, which gives an estimation of Debye length of  $\lambda_{D,w} \simeq 10$  nm  $\ll H$ . The interface charging parameters are obtained through fitting process using a single phase electrokinetic model with no-slip boundary at the air-water interface, giving  $\zeta_{sl} = -110$  mV and  $\sigma_{lg} = -0.17$  C/m<sup>2</sup>, as the blue dot-dash line in Fig. 3 shows, where the distance from the bottom  $h$  is nondimensionalized using the characteristic depth of  $H_0 = 1$  mM. The  $\zeta$  potential at the air-water interface is then calculated through the Grahame's equation, the value of which is about  $-230$  mV, coinciding with the results in the previous papers [68].

In the diffuse-interface based modeling, the system setup is essentially the same as Fig. 1, where liquids 1 and 2 are replaced by the air and water phases, respectively. To mimic a closed cell (for liquid 2),  $\Delta p$  is nonzero and adjusted to satisfy the zero total mass flux condition in the plane-interface techniques. To mimic the fixed boundary at the air-water interface, the dynamic viscosity of the upper (artificially *solidified*) air phase is assumed to be a thousand times of the lower water phase which induces a large viscosity ratio  $\mu_r = 1000$  between the upper and lower phases, along with the permittivity ratio  $\varepsilon_r = 1/80$  and density ratio  $\rho_r = 1/1000$ . The interface charging parameters including  $\zeta_{sl}$  and  $\sigma_{lg}$  are determined by fitting the experimental results as aforementioned. The artificial upper boundary for the *solidified* air phase is assumed no-slip with  $\zeta_{sg} = 0$  mV, and the specific value of  $\zeta_{sp}$  has little influence on the fitting parameters for that the ions are completely depleted in the air phase, whose free energies of transfer are set to  $\mathcal{G}_{t,\pm} = 300$ . For convenience in the numerical simulation,  $H$  is set to 10  $\mu$ m without loss of generality which has little influence on the following analysis considering the electrokinetic phenomena is determined by

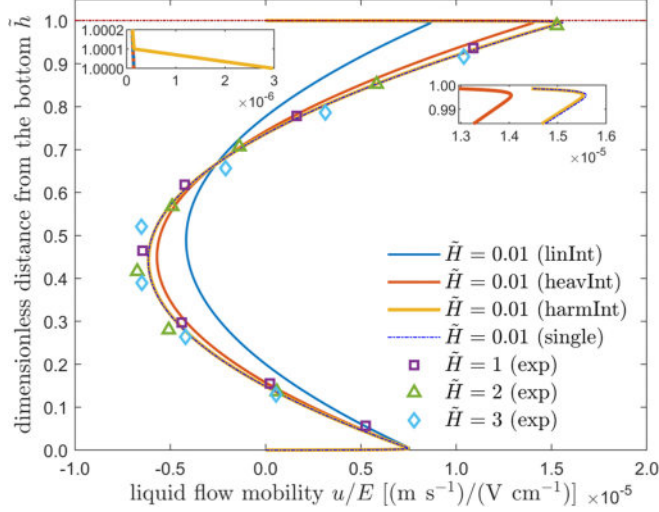


FIG. 3. Validation against the experimental results of the plane-interface methods. The upper boundary of the open cell is denoted by the black dash line, and the upper boundary of the artificial air phase in the diffuse interface simulation is denoted by the red dash line. The results are expressed in the dimensionless distances from the bottom which are rescaled using the total depth  $H$  of the channel. The results from PIV experiments are denoted as different symbols, which almost lay in the same dimensionless velocity profile, suggesting the linearity of the air-water electroosmosis phenomena. The profile has been fitted using a single phase electrokinetic model assuming the no-slip boundary at the air-water interface due to the solidification effect of ionic surfactants, as the blue dot-dash line shows, with  $\zeta_{sl} = -110$  mV and  $\sigma_{lg} = -0.17$  C/m<sup>2</sup>. The results with the linear, heaviside, and harmonic interpolation of dynamic viscosity are denoted by blue, red, and orange solid lines, showing that the consistency between the physical model results and the experimental results is strongly dependent on the choice of interpolation strategy of viscosity.

the ion-fluid coupling transport within the nanoscale diffuse layer region. Besides,  $d'_{ad}$  in Eq. (10) is set to zero which ensures the same net charge distribution at the air-water phase as the single phase electrokinetic model, and the prescribed surface charge density  $\rho_{fix}(\phi)$  in Eq. (12) is accordingly changed to  $\sigma_{ll}/d_{pf}$  within the region  $\tilde{\phi}(0) < \phi < \tilde{\phi}(d_{pf})$ .

Following the verification part, we first utilize the linear interpolation strategy for the dynamic viscosity model  $\mu(\phi)$ , whose simulation results are shown as the blue solid line in Fig. 3. It is clearly seen that the electroosmotic velocity at the air-water interface is severely underestimated due to the overlarge viscosity value in the vicinity of air-water interface, especially the diffuse layer region, where the viscous resistance against the electroosmotic force is amplified due to the artificially large viscosity induced by the linear interpolation and the velocity is thus reduced.

With the same interface charging parameters, different interpolation strategies of  $\mu(\phi)$  are then tested, including the linear, heaviside, and harmonic interpolation functions as follows:

$$\begin{aligned}
 \mu_{lin}(\phi) &= \phi_w \mu_w + \phi_a \mu_a, \\
 \mu_{heav}(\phi) &= \mu_w + (\mu_a - \mu_w)H(\phi_a - 0.5), \\
 \mu_{harm}(\phi) &= \frac{1}{\phi_w/\mu_w + \phi_a/\mu_a},
 \end{aligned} \tag{21}$$

where  $\phi_\alpha$  is the local volume fraction of phase  $\alpha$  defined in Eq. (1), and  $H(x)$  is the Heaviside function taking the value of 1 for  $x > 0$ , and 0 for  $x \leq 0$ . The results of the three interpolation strategies are shown as the solid lines in Fig. 3. It is shown the latter two interpolation functions agree well with the single phase results, signifying that quite different interfacial charging

parameters may be obtained if different interpolation functions for viscosity are used. There have been several discussions on the reason why harmonic interpolation leads to a better performance of velocity profile prediction, such as continuity of shear stress, improved accuracy of flux balance, and independence of diffuse layer thickness [69–71].

The results suggest that with regard to the experimental results for the fluid-liquid interfacial electrokinetic flow, if the material property ratio is large and the diffuse layer thickness is comparable with the solvent mixing layer (which is commonly satisfied in practice), the detailed material property distribution is essential in the theoretical interpretation and may reconcile the contradictory results in the interpretation of velocity profiles in previous studies [68]. In fact, it is always an important issue to optimize the material property interpolation scheme either to achieve a better numerical stability for the lattice Boltzmann model [72,73], or to improve the accuracy compared with the sharp interface model in volume-of-fluid models [74,75]. However, different from the aforementioned models concerning the numerical performance, the material property interpolation strategy discussed here is directly related to the physical picture underneath the fluid-liquid interfacial electrokinetic flow rather than merely a numerical issue, which has been discussed in several previous studies [76,77].

### B. Impurity and permittivity effects in interfacial electrokinetics: Ion partitioning effect

In this subsection, the real charged interface systems are considered to study the interplay of the two possible charging mechanisms for different types of organic liquids and various concentrations of impurity ions, and approach (B) is utilized to include either Born potential model or nonlocal electrostatics model linking partition coefficients to the permittivity ratio and charged species as well as the linear adsorption isotherms connecting the bulk ionic concentration and interface charge density.

As aforementioned, the nonpolar organic liquid and polar organic liquid may show quite different charging mechanisms due to their distinct permittivities; therefore, both of the two types of organic liquid phases are considered here. The constituent ions similar to KCl used for conductivity calculation are prioritized, and the specific type of organic liquid phase is chosen in such way that the data of free energies for ions through the resultant two-liquid interface is available. To be specific, the electrolyte KCl in water are chosen as support electrolyte with  $[\text{Ph}_4\text{As}]\text{Cl}$  in organic liquid as model impurity ion, and *n*-decane and nitrobenzene are chosen as the nonpolar organic liquid and polar organic liquid, respectively. The Gibbs free energies utilized here are listed below:

$$\begin{aligned} \mathcal{G}_{\text{a,OH}^-} &= -25, & \mathcal{G}_{\text{a,others}} &\simeq 10 \gg 1, \\ \mathcal{G}_{\text{t,OH}^-}^{(\text{np})} &= 471.05, & \mathcal{G}_{\text{t,OH}^-}^{(\text{p})} &= 18.45, \\ \mathcal{G}_{\text{t,H}^+}^{(\text{np})} &= 353.65, & \mathcal{G}_{\text{t,H}^+}^{(\text{p})} &= 7.51, \\ \mathcal{G}_{\text{t,K}^+}^{(\text{np})} &= 533.96, & \mathcal{G}_{\text{t,K}^+}^{(\text{p})} &= 5.47, \\ \mathcal{G}_{\text{t,Cl}^-}^{(\text{np})} &= 464.26, & \mathcal{G}_{\text{t,Cl}^-}^{(\text{p})} &= 18.66, \\ \mathcal{G}_{\text{t,Ph}_4\text{As}^+}^{(\text{np})} &= 244.80, & \mathcal{G}_{\text{t,Ph}_4\text{As}^+}^{(\text{p})} &= -16.75. \end{aligned}$$

For the detailed values and estimation process of the material properties, please refer to Appendix D. Particularly, the  $\text{Ph}_4\text{As}^+$  ion is seen to be preferable to reside in water rather than *n*-decane due to the extremely low permittivity of this nonpolar organic liquid, compared with the nitrobenzene-water interface where the impurity ion tends to stay in the polar organic liquid phase. It should be noted that this conclusion comes from the nonlocal electrostatics method, which only includes the electrostatic force and interface tension effect between two solvent phases, while the detailed nonelectrostatic interaction between organic ion and solvent molecules may be not fully accounted for, such as the van der Waals force and steric effect.

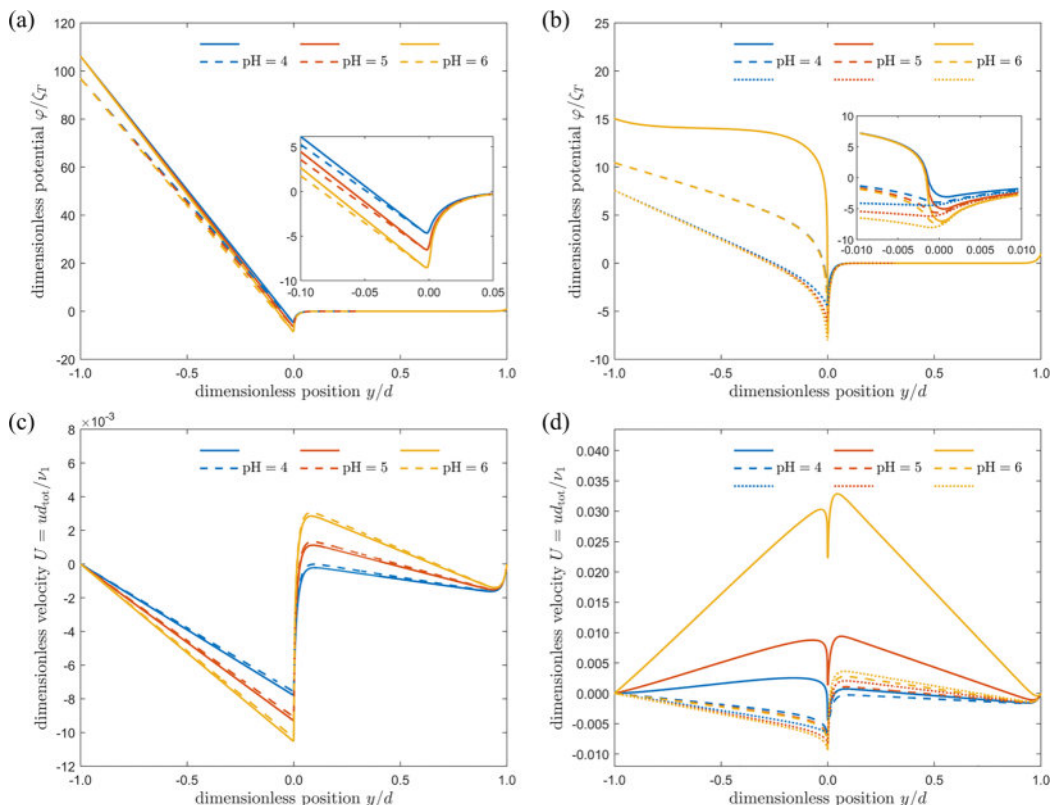


FIG. 4. Dimensionless electric potential and velocity profiles for  $n$ -decane ( $\varepsilon_0^{(np)} = 2\varepsilon_0$ ) and nitrobenzene ( $\varepsilon_0^{(p)} = 35\varepsilon_0$ ). The results for the former nonpolar organic liquid are shown in panels (a) and (c), with those for the latter polar organic liquid in panels (b) and (d). The material property ratios and the Gibbs free energies are referred to Sec. III B. For nonpolar organic liquid [panels (a) and (c)], the solid and dash lines are results for  $pOrg_w = 7$  and  $15$ , respectively. For polar organic liquid [panels (b) and (d)], the solid, dash, and dotted lines are results for  $pOrg_o = 5, 7$ , and  $15$  (corresponding to  $pOrg_w \simeq 6.2, 10.2$ , and  $19.4$ ), respectively.

We choose  $c_{H^+,w}$  and  $c_{Cl^-,w}$  as well as  $c_{Ph_4As^+,w}$  ( $c_{Ph_4As^+,o}$ ) as the independent variables for the cases of nonpolar (polar) organic liquids, respectively. Hydroxyl ion  $OH^-$  acts as the potential determining ion in the specific adsorption process, and the cases with  $3 < pH < 6.5$  in water phase are investigated where the specific adsorption of  $OH^-$  can be approximated as a linear isotherm [22]. The ionic strength  $I_w$  takes the value of 1 mM, which gives  $c_{Cl^-,w} = 1$  mM. Note that here the concentration of impurity ion is chosen to be much less than 1 mM and its impact on interface tension can be safely ignored. Besides, the impurity ion is assumed to be inert here, and thus the possible chemical reaction between  $Ph_4As^+$  and other ions such as  $Cl^-$  is ignored. The dimensions of the straight channel and initial configuration of liquid phases are  $d_{tot} = 1 \mu m$  and  $d_1 = d_2 \equiv d = d_{tot}/2$ , without loss of generality. The  $\zeta$  potentials at solid boundaries are set to  $\zeta_1 = \zeta_2 = \zeta_T$  as before. The simulation results for the nonpolar and polar organic liquids as well as the corresponding essential characteristic system properties are shown in Fig. 4.

As shown in Figs. 4(a)–4(d), the major difference between the nonpolar and polar organic liquids lies in the sensitivities to the impurity ions and the interplay of the two charging mechanisms. To be specific, the interfacial charging and electrokinetic flow behaviors of the nonpolar two-liquid interface are seen to be insensitive to the impurity ion (between  $pOrg_w \equiv pPh_4As_w = 7$  and  $15$ ) under different pHs, while those for the polar organic liquid show obvious discrepancies (among

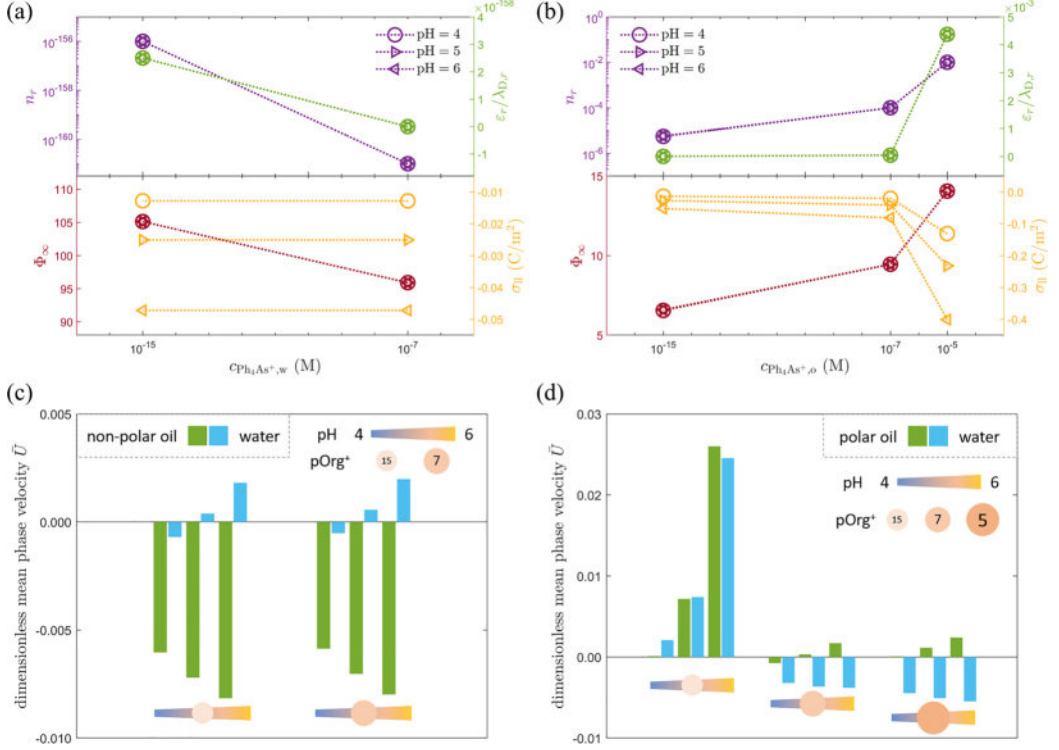


FIG. 5. Dimensionless characteristic properties and phase mean velocities for  $n$ -decane ( $\varepsilon_0^{(\text{np})} = 2\varepsilon_0$ ) and nitrobenzene ( $\varepsilon_0^{(\text{p})} = 35\varepsilon_0$ ). The results for the former nonpolar organic liquid are shown in panels (a) and (c), with those for the latter polar organic liquid in panels (b) and (d). The material property ratios and the Gibbs free energies are referred to Sec. III B. In panels (c) and (d), the results for different pHs are denoted by the different symbols, while the dotted lines are only guides for eyes.

$p\text{Org}_0 \equiv p\text{Ph}_4\text{As}_0 = 6.2, 10.2, \text{ and } 19.4$  for each pH. This originates from the large permittivity ratio between water and nonpolar organic liquid which almost depletes the ions inside the organic liquid phase, i.e.,  $n_r \ll 1$ , resulting in a rather large  $\lambda_{D,o}^{(\text{np})}$  and making it essentially behave as the dielectrics depicted in Figs. 4(a) and 4(c). On the contrary, for the polar organic liquid, the permittivity ratio is not large and the screening effect within the organic liquid phase may still play an important role, and the ionic concentration ratio  $n_r$  is thus sensitive to the impurity ions which triggers the transition from an interface between dielectrics and strong electrolyte solution, to the one between two immiscible electrolyte solutions (ITIES), which leads to completely different electrokinetic behaviors, as shown in Figs. 4(b) and 4(d). With regard to the interplay of the charging mechanisms, it is seen from Fig. 4(d) that the influence of pH for the nonpolar organic liquid case is monotonic for each impurity ionic concentration, while it is rather complicated for the polar organic liquid case. Since we have excluded the chemical-reaction-induced mechanism, the specific adsorption mechanisms underneath for the two types of organic liquids should not differ much with each other. This indicates that it is the differences in partition-induced interface charging that lead to the distinct two-liquid electroosmotic flow behaviors.

In fact, the diffuse layer capacity ratio  $\varepsilon_r/\lambda_{D,r}$  determines the partition of the potential drop in each phase from the total distribution potential across the two bulk phases [78]. We calculate this ratio for different organic liquids and system setups [as shown in the upper box and right y axis of Figs. 5(a) and 5(b)]. It is found that the nonpolar organic liquid presents an extremely low value which retains most of the distribution potential within the organic liquid phase, contributing

the negligible charge imbalance between the two electrical diffuse layers induced by the ion partitioning. As a result, though the distribution potential  $\Phi_\infty$  for the nonpolar organic liquid is rather large (compared with the thermal potential  $\zeta_T$ ), the interface charge density  $\sigma_{\text{II}}$  shows an impurity-insensitive sub-linear scaling on the concentration of potential-determining ion and the electrokinetic behavior is determined by the specific adsorption mechanism, as shown in the lower box of Fig. 5(a). In contrast, for the polar organic liquid case, the double layer capacity ratio is much larger than the nonpolar organic liquid's [as shown in the upper box and right y axis of Fig. 5(b)], which indicates a greater influence of the imbalanced distribution potential on the interfacial charge imbalance of the two electrical diffuse layers. The lower box of Fig. 5(b) depicts the partition-induced distribution potential  $\Phi_\infty$  and specific adsorption-induced interface charge density  $\sigma_{\text{II}}$ . It is shown that when the impurity ion concentration is low, the interface charge density is similar to that of nonpolar organic liquid, while for high concentration of impurity ions, the interfacial charge will increase to a great extent due to the amplification effect of distribution potential. It should be pointed out that in the cases of impurity ions with high concentration, the large values of surface charge density indicate that the ionic correlation such as steric effect may be indispensable, which requires further study but will not change the basic qualitative observations here and below.

The most striking and complex phenomena occur in the polar organic liquid case. To illustrate the dependence of velocity profiles on the solutions properties such as pH and impurity ion concentration more clearly, we plot the phase mean velocities in the case in Figs. 5(c) and 5(d). Though the variation of potential profile is monotonic on pH and impurity concentration [Fig. 4(b)], it is shown in Fig. 5(d) that there exists a nonmonotonic dependence of the flow rate within the water phase on the impurity concentration, as well as the pH-dependent symmetry evolution of the flow rate at the two sides of two-liquid interface. It is relatively straightforward to give an explanation of the latter effect, i.e., the pH-dependent symmetry evolution of the flow rate. Specifically, when the pH increases while the impurity ion maintains a constant, the specifically adsorbed ion at the two-liquid interface (which is the hydroxyl ion  $\text{OH}^-$  here) will increase, and the water side which has a larger double layer capacity [Fig. 5(d)] will acquire a greater number of ions and thus shows a higher electroosmotic velocity than the organic liquid phase. With regard to the nonmonotonic dependence of water velocity on the impurity concentration, it essentially comes from the competition effect between the two charging mechanisms. When the concentration of impurity ions increase from a tiny value, the distribution potential as well as its partition in the organic liquid phase increases while the adsorption induced interface charge exhibits minimal variation [Fig. 5(d)], which enhances the electroosmosis flow in the organic liquid phase and leads to a decrease of the velocity in the water phase; however, if the impurity ion concentration continues to increase and becomes high enough, the adsorption-induced interface charge will increase [Fig. 5(b)], and considerably raise the water velocity against the attenuation effect caused by the distribution potential increase. These results reflect that the complex interplay between the two charging mechanisms when the permittivity of the two liquids are close to each other, even if the organic ion concentration is not large enough to form an ITIES system, which provides alternative perspectives in comprehending the two-liquid electrokinetic phenomena and offers rich possibilities for future applications.

It should be pointed out that the dependencies of solid surface charge, interface tension coefficient and contact angle on the bulk ionic concentration are ignored through this work. Besides, considering that the additional Gibbs free energy profile is defined as a single-variable function of the phase order parameter in this work, it is assumed that the ion distribution normal to the two-liquid interface due to the interphase transfer and interface adsorption does not depend on the other local fields such as ion concentration and velocity, suggesting that the specific adsorption coefficient will have a *uniform* distribution along the two-liquid interface. If the double layers of solid boundary and two-liquid interface overlap or there is a large tangential gradient of ion concentration, the charge regulation boundary instead of the constant potential or surface charge boundary at the solid surface will be required [11], while a nonuniform specific adsorption coefficient at the two-liquid interface will also need to be determined based on the local concentration [48,79]. In addition,

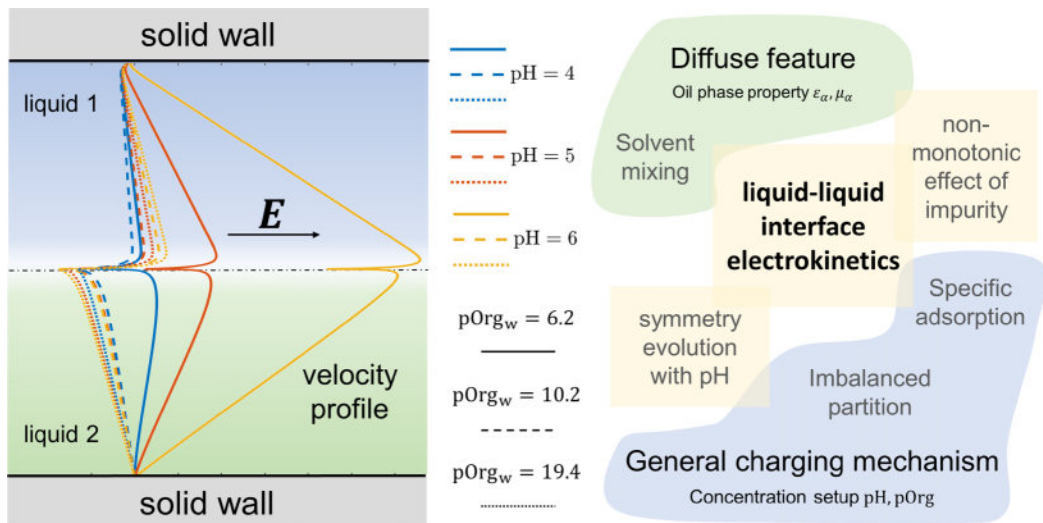


FIG. 6. Schematics highlighting the essential features of the framework in this work.

$d_{pf} \equiv \sqrt{2\epsilon_{pf}} \lesssim \lambda_{D,\alpha}$  is satisfied in this work and thus the influence of the variations in the detailed ionic distribution within the solvent mixing layer can be safely ignored; otherwise, when the two scales  $d_{pf}$  and  $\lambda_{D,\alpha}$  are comparable, the complex microscopic interaction within nano-scale solvent mixing layer of two-liquid interface and strong screening from local free charges may be significant due to the nonuniform permittivity, which is beyond the scope of this work. It is also noteworthy that since the smallest system scale in this work is around  $1 \mu\text{m} \gg 10 \text{ nm}$ , the van der Waals force between the surfaces and interfaces is unimportant; otherwise, its impact on the interface movement should be incorporated into the Cahn-Hilliard-Navier-Stokes equations for the evolution of the two-liquid interface through such as lubrication theory or fluctuating hydrodynamics [80,81], which needs further studies.

#### IV. CONCLUSIONS AND PERSPECTIVES

The spontaneous charging of immiscible liquid-liquid interface plays a fundamental role in the stability and self-organization behaviors of colloidal system and its electrokinetic flow behaviors exist in various fields, such as suppressing viscous fingering by triggering the electrokinetic flow using external electric field [82]; curvature or thickness tuning of liquid film for optical lens or nano sensor [83,84]; and imbibition process alteration in nanoporous media benefiting from electrowetting [85]. The solvent mixing effect, which has been primarily considered in the liquid-liquid electrochemistry field, have not been well understood yet when it comes to the electrokinetic flow, where the potential drop and viscosity transition within the solvent mixing layer may be essential. Besides, the two major charging mechanisms (imbalanced partition and specific adsorption) of the two-liquid interfacial systems have only been individually studied and their interplay remains uncovered yet, which should have been commonly met in those systems with organic ionic impurities.

In this contribution, we propose a unified framework based on the diffuse interface model and modified Boltzmann formulation to investigate the aforementioned effects in the two-liquid (two-liquid) interfacial charging and electrokinetic flow, in which the interface charging characteristic parameters are determined by the physicochemical properties and ionic concentration setups in the real systems, serving as the constitutive relationship of two-liquid interface charging, as shown in Fig. 6. Our work shows the necessity of utilization of a diffuse interface model incorporated with the detailed charging mechanisms in dealing with the two-liquid electrokinetic multiphase

flow problem, and provides a promising framework for the further exploration of problems, such as electrophoresis and electrocoalescence of biological cells [86–89], ion-assisted regulation of wettability and contact line dynamics [90–93], and organic liquid ganglia evolution in confined media under electric field [94–96].

The solvent mixing effect is first addressed by comparison with the theoretical solution of the sharp interface model, in which we utilize a complete set of interfacial charging parameters compared with the previous studies [35], i.e., distribution potential  $\Delta_w^o\varphi_\infty$ , interface surface charge  $\sigma_{il}$ , and solvent mixing layer potential drop  $\Delta_w^o\varphi_i$ , for which a semiempirical correction formula is proposed for its practical utilization. The proposed diffuse-interface model has been compared with the experimental results from the plane-interface technique, which is used to measure the air-liquid interfacial charging density. It is shown that for an two-liquid interface with a large viscosity ratio, the viscosity interpolation model  $\mu(\phi)$  is demonstrated to have a great impact on the interpretation of the quantitative dependence of electroosmosis velocity profile on its interface charging. This indicates that the essentially diffuse feature may have profound influence on the theoretical foundation of electrokinetic measurements of two-liquid interfacial charging and may reconcile the previous discrepancies on its interface charging, on which more attention needs to be paid [26,68].

Compared with the previous studies focusing on the adsorption-induced surface charging [22,59], the interplay of the two charging mechanisms in practical systems is studied for the first time, through effects of impurity ions and permittivity of the organic liquid phase. The major difference between the nonpolar and polar organic liquids lies in the sensitivities to the impurity ions, as well as the competition effect between the two charging mechanisms which is significant only when the permittivity ratio is moderate (about  $\varepsilon_r \simeq 1/2$ ). The underneath mechanisms of the pH-dependent symmetry evolution of the velocity profile and the nonmonotonic dependency of the water velocity on the impurity concentration are exhaustively discussed, and attributed to the dependency of the interface charging state on the physicochemical conditions such as impurity ion concentration and pH. This will promote the studies on the self-propelled droplet design and cell taxis mechanism in biophysics [86,97–100], nonintrusive self-potential subsurface detection in geophysics [101], and liquid-infused-structure-based energy-harvesting in power engineering [20], in which the constitutive relationship of two-liquid interface charging may be vital.

#### ACKNOWLEDGMENTS

The authors thank the anonymous referee who provided useful and detailed comments on the manuscript. This work was financially supported by the National Natural Science Foundation of China (Grant No. 12272207) and the National Key R&D Program of China (Grant No. 2019YFA0708704).

#### APPENDIX A: A BRIEF OVERVIEW OF TWO-LIQUID INTERFACIAL CHARGING MECHANISM

Generally speaking, for a certain immiscible two-liquid solvent interface and charged ion as the solute, both polarizability and adsorbability are related to the interaction between the solute ions and solvent molecules. The former describes whether the solute tends to pass the solvent interface freely under external field which is related to the ion partition behavior and the Gibbs free energy of transfer as an overall difference between the bulk regions of two phases, while the latter here reflects whether the solute tends to be specifically adsorbed into the interfacial region which is related to the ion adsorption behavior and the Gibbs free energy of specific adsorption as an average of the solvent mixing layer region. It is noteworthy that to obtain a complete description of the interface charging behavior, it is required to provide the *detailed profiles* of additional Gibbs free energy instead of these two *overall differences* from a rough classification of the interphase partition and interface adsorption behaviors of ions, which are indeed intrinsically linked to the complex detailed specific

interactions between solute ions and solvent molecules as well as the other ions within and around the solvent mixing layer region.

It is noteworthy to point out that the distribution potential is often used to character the partition-induced charging, while the interface charge density is utilized as the characteristic quantity for adsorption-induced charging. Besides, for the two-liquid interface with no ionizable sites and simple ions, the free energy of transfer is highly sensitive to the specific characteristics of charged species *and* the organic liquid permittivity, while the free energy of ion adsorption is closely related to the property of solute ion *but* is almost independent on the organic liquid permittivity. Here we focus on the overall (average) description in a thermodynamic manner, while the detailed profiles with possible kinetic and electrostatic effects will be introduced in Sec. II B.

Ion partition between adjacent liquid phases is related to the free energy of transfer of single solute ion  $i$  from phase  $\alpha$  to phase  $\beta$  denoted by  $\Delta_{\alpha}^{\beta} g_{t,i}^0 = \mu_i^{0,\beta} - \mu_i^{0,\alpha}$ , which can be written in the form of characteristic electric potential and  $\beta$ - $\alpha$  partition coefficient,

$$\Delta_{\alpha}^{\beta} g_{t,i}^0 \equiv -z_i e \Delta_{\alpha}^{\beta} \varphi_i^0 \equiv -k_B T \ln P_i^{\beta/\alpha}. \quad (\text{A1})$$

To illustrate the essential physics, let us consider an interface system with single pair of solute ions, and ignore the effects of complex species formulation, selective permeability and redox-reduction reaction. From the equilibrium of electrochemical potential of each solute as well as the electrically neutral condition in the bulk region of each liquid phase, it is obtained that

$$\begin{aligned} \Delta_{\alpha}^{\beta} \varphi_{\infty} &\equiv \varphi_{i,\infty}^{(\beta)} - \varphi_{i,\infty}^{(\alpha)} = \frac{\Delta_{\alpha}^{\beta} \varphi_{+}^0 + \Delta_{\alpha}^{\beta} \varphi_{-}^0}{2} \\ &= -\frac{\Delta_{\alpha}^{\beta} g_{t,+}^0 - \Delta_{\alpha}^{\beta} g_{t,-}^0}{2e}, \end{aligned} \quad (\text{A2})$$

and

$$\begin{aligned} n_r &\equiv \frac{n_{i,\beta}}{n_{i,\alpha}} \simeq \frac{a_{i,\beta}}{a_{i,\alpha}} = P_i^{\beta/\alpha} \exp\left(-\frac{z_i e}{k_B T} \Delta_{\alpha}^{\beta} \varphi_{\infty}\right) \\ &= \sqrt{P_{+}^{\beta/\alpha} P_{-}^{\beta/\alpha}} \equiv \exp\left(-\frac{\Delta_{\alpha}^{\beta} g_{t,+}^0 + \Delta_{\alpha}^{\beta} g_{t,-}^0}{2k_B T}\right). \end{aligned} \quad (\text{A3})$$

Here we only give the results of 1:1 electrolytes (whose constituent ions are denoted by  $i = \pm$ ), which could be easily extended to more complex cases. In Eqs. (A2) and (A3),  $\Delta_{\alpha}^{\beta} \varphi_{\infty}$  denotes the equilibrium distribution potential between the bulk phases,  $a_{i,\alpha(\beta)} \equiv a_{i,\infty}^{\alpha(\beta)}$  and  $n_{i,\alpha(\beta)} \equiv n_{i,\infty}^{\alpha(\beta)}$  denote the activity and concentration of ion  $i$  within the bulk and electrically neutral region of phase  $\alpha(\beta)$ , respectively, and the activity coefficients are assumed to satisfy  $\gamma_{+}^{(\alpha)} \gamma_{-}^{(\beta)} \simeq \gamma_{-}^{(\alpha)} \gamma_{+}^{(\beta)}$ . It is indicated that both equilibrium potential difference and ionic concentration ratio depend on the free energy of transfer of solute ions, whose specific value can be measured through electrochemical techniques such as the cyclic voltammetry method and choosing a certain ion pair as the reference point of  $\Delta_{\alpha}^{\beta} g_{t,i}^0$ . It should be noted that the value of partition coefficient is dependent not only on the solvents themselves, but also on the solute ions.

For simple metal and halide ions, the permittivity of organic liquid is usually smaller than the water's, thus the two-liquid partition coefficient is much less than 1, and the typical values of free energy of transfer are around  $3 - 9k_B T$  [102]. Compared with those nonpolar organic liquids whose low-frequency permittivity is extremely lower than water (usually less than  $5\epsilon_0$ ), there will be more (but still very few) ions in the water phase entering the polar organic liquids whose low-frequency permittivity is smaller than water but takes a moderate value (usually around  $30\epsilon_0$ ). For organic ions with phenyl group, long alkyl chain, or chelated benzene ring, they are preferable to reside in the organic liquid phase, resulting in an two-liquid partition coefficient much larger than 1. Theoretically, the free energy of transfer can be roughly estimated using the Born potential which only considers the local linear electrostatic effect and tends to extensively overestimate the

free energy of solvation thus induce significant errors. A more accurate model is called nonlocal electrostatics model, which includes the nonlocal electrostatic and solvophobic effects [32]. In this work, we compare the Born potential model with the nonlocal electrostatics theory and use the latter to investigate the permittivity dependence of ion partition.

Depending on the types of solvent molecule and solute ion, the underneath specific mechanism adsorbing the ions from the bulk phase to the interface varies from case to case, such as hydration/dehydration, amphiphilic structure, hydrogen bonding, or chemical reaction. On the one hand, for ionic surfactants, the adsorption isotherm is usually used to describe the potential dependence of the adsorbed amount. This approach has been used in the electrochemical instability studies [57], in which the linear variation of the *total* adsorption Gibbs energy on the distribution potential is assumed:

$$\begin{aligned}\Delta_{\alpha}^i g_{a,i}^{\text{total}} &= \Delta g_{a,i}^0 + \beta_i k_B T y_i, \\ \Delta_{\beta}^i g_{a,i}^{\text{total}} &= \Delta g_{a,i}^0 + (\beta_i - 1) k_B T y_i.\end{aligned}\quad (\text{A4})$$

The Frumkin isotherm is used to describe the adsorption saturation as well as the in-plane interaction behavior,

$$K_{a,i}^{\text{eff}} a_{i,\alpha} \equiv f(\theta_i) = \frac{\theta_i}{1 - \theta_i} e^{-2a_F \theta_i}, \quad (\text{A5})$$

and then the thermal equilibrium of the adsorption and partition processes is expressed as follows:

$$\frac{K_{a,i} m_i e^{(1-2\beta_i)y_i}}{V^{\alpha} e^{-\beta_i y_i} + V^{\beta} e^{(1-\beta_i)y_i}} = f(\theta_i). \quad (\text{A6})$$

Here,  $\Delta g_{a,i}^0 = \Delta_{\alpha}^i g_{a,i}^0 = \Delta_{\beta}^i g_{a,i}^0$  is the assumed symmetric Gibbs energy of the *specific* adsorption of solute ion  $i$  from both phases to the interface at  $\Delta_{\alpha}^{\beta} \varphi_i^0$ ,  $\beta_i$  is a kinetic constant that is independent on  $\Delta_{\alpha}^{\beta} \varphi$ ,  $y_i = (z_i e / k_B T) (\Delta_{\alpha}^{\beta} \varphi - \Delta_{\alpha}^{\beta} \varphi_i^0)$ ;  $\theta_i$  is the surface coverage of ion  $i$ ,  $K_{a,i}^{\text{eff}}$  is the effective *total* adsorption coefficient of  $i$ , and  $a_F$  is the interaction parameter;  $K_{a,i} = \exp(-\Delta g_{a,i}^0 / k_B T)$  is the *specific* adsorption coefficient of  $i$  at  $\Delta_{\alpha}^{\beta} \varphi_i^0$ ,  $m_i$  is the total amount of the surfactant  $i$  in the system, and  $V^{\alpha(\beta)}$  are the volume of the phases  $\alpha(\beta)$ , respectively. The above mechanism suggests that the electrochemical driving force for the asymmetric adsorption from each phase is a fixed fraction of the distribution potential, incidentally resembling the Butler-Volmer equation in reactive electrode.

On the other hand, for simple ions such as metal ions and halide ions, the specific adsorption mechanism is case-by-case. For those polar organic liquids with surface ionic groups such as crude organic liquids, the mechanism is usually named as ionization of surface groups described by the surface complexation model, which is characterized by the equilibrium constants of surface chemical reactions and free energy of possible dehydration process [103]; while for those organic liquids with no ionizable sites at the pristine interface, the mechanism is still unclear and under debate, in which the most acknowledged mechanism is the hydroxyl adsorption described by the Stern adsorption isotherm and the adsorption free energy may be related to the hydrogen bonding [22]. A typical characteristic of its interface charging is the commonly shared behavior of their quantitatively similar dependence on the bulk concentration and pH among various types of nonpolar organic liquids, such as decane, hexadecane, and xylene [22,104]. In this work, we focus on the two-liquid interface systems with simple ions but no ionizable interface sites and utilize the linear adsorption isotherm as the dilute limit of those complicated complexation or isotherm formulations.

## APPENDIX B: PERTURBATION APPROACH OF ELECTROKINETIC MULTIPHASE FLOW AND TRANSPORT

Herein, to acquire a general approach, the perturbation method will be utilized which can be directly extended to more complex situations where the normal component of external electrical

field at the interface is nonzero and the material property variation across the interface regulates the local electric field. We will illustrate its physical rationale and then give its mathematical formulation in this part.

Generally speaking, the main difference between electrokinetics and electrohydrodynamics is the origin of interface charge imbalance. To be specific, the former focuses on the kinetic origin induce by interfacial physicochemical effects under relatively weak external electric field in strong electrolyte solution, while the latter centers on the electrodynamic origin induced by the ion/electron transport under relatively strong external electric field in dielectric liquid or weak electrolyte solution. In general, a strong electrolyte solution with a molar concentration between  $10^{-5}$  M and  $10^{-1}$  M in a certain solvent (saying the water) whose activity coefficient is nearly 1 permits a much thinner diffuse layer and higher local electric field compared with solutions with low conductivity such as weak electrolyte solutions treated in induced-charge electrohydrodynamics. Thus, the internal electric field near a spontaneously charged interface is scaled around  $1 \times 10^6$  V/m, while the imposed external electric field utilized in electrokinetic manipulation is usually less than  $1 \times 10^4$  V/m. Thus, it is quite reasonable to consider the influence of small external electric field as a perturbation  $\delta\varphi$  to the electric field of the equilibrium charge distribution  $\varphi^{\text{eq}}$  at each moment of phase evolution, and ignore the field-induced interface charge as well as the ensuing electrohydrodynamic and electrowetting effects.

A rigorous treatment of ion transport requires the combination of Poisson equation (7) with the following Maxwell-Stefan equation

$$\frac{\partial n_i}{\partial t} + \nabla \cdot (n_i \mathbf{u} + \mathbf{J}_i^{**}) = 0, \quad (\text{B1})$$

where  $\mathbf{J}_i^{**}$  is the number flux of ion  $i$  in the following potential form

$$\begin{aligned} \mathbf{J}_i^{**} &\equiv -\tilde{D}_i n_i \frac{\nabla \mu_i}{k_B T} \\ &= -\tilde{D}_i (\nabla n_i + n_i \nabla \ln \gamma_i^\phi + n_i \nabla \ln \gamma_i^\varphi), \end{aligned} \quad (\text{B2})$$

where  $\mu_i = \mu_i^0 + k_B T \ln(\gamma_i^\phi \gamma_i^\varphi x_i)$  is the chemical potential of ion  $i$  with the number fraction  $x_i$  and volume number density  $n_i$  in the mixture. Here,  $\tilde{D}_i$  is the local Maxwell-Stefan diffusion coefficient of ion  $i$  which along with the dynamic viscosity  $\bar{\mu}$  is dependent on the local number fraction  $x_i$  according to the Stokes-Einstein-Onsager relation, and  $\gamma_i^\phi, \gamma_i^\varphi$  are the effective activity coefficients defined by

$$\gamma_i^\phi := \exp\left(\frac{\Delta g_i(\phi)}{k_B T}\right), \quad \gamma_i^\varphi := \exp\left(\frac{z_i e \varphi}{k_B T}\right), \quad (\text{B3})$$

which are induced by the additional Gibbs free energy  $\Delta g_i(\phi)$  and electric potential  $\varphi$ , respectively. Equation (B1) can be written into a more familiar form, i.e., the *modified* Nernst-Planck equation of ion transport

$$\frac{\partial n_i}{\partial t} + \nabla \cdot \left( n_i \mathbf{u} - \tilde{D}_i (\nabla n_i + n_i \nabla \ln \gamma_i^\phi) - \frac{z_i e \tilde{D}_i}{k_B T} n_i \nabla \varphi \right) = 0, \quad (\text{B4})$$

in which the additional free energy term has been added into the original Nernst-Planck equation, and  $\tilde{D}_i \equiv \tilde{D}_i$  for which the nonideal solution effect is ignored and the specific form will be given below. Now, the Eqs. (2), (5), and (B4), along with the necessary boundary conditions, provide a complete description of the electrokinetic multiphase flow system. For convenience, here we only consider a boundless domain where only the water phase can extend to infinity, i.e.,  $\phi_\infty = -1$ . Besides, at every point of the far field boundary, the ion concentration and electric field are both constant and uniform (denoted by  $n_{i,\infty}$  and  $\mathbf{E}_\infty$ , respectively), and the total fluid stress is zero. It is straightforward to modify the following discussions to accommodate more complex boundaries such

as charged solid wall with the prescribed excess surface charge, metal electrode with the prescribed electrical potential, periodic two-liquid interface extending to the infinity, and three-phase contact line with the prescribed contact angle.

Since the disturbance of electric potential and ion concentration field triggered by external electric field is small, following the traditional process of perturbation for single-phase electrokinetics, the unperturbed state of the multiphase electrokinetic system at each time step is assumed as the equilibrium distribution of electric potential and ion concentration with prescribed additional Gibbs free energy corresponding to the transient phase distribution  $\phi(t)$  and a quiescent velocity field  $\mathbf{u}^{\text{eq}}(t) = 0$ , i.e.,

$$\begin{aligned}\varphi &= \varphi^{\text{eq}} + \delta\varphi, & n_i &= n_i^{\text{eq}} + \delta n_i, \\ \mathbf{u} &= \mathbf{0} + \delta\mathbf{u}, & p &= p^{\text{eq}} + \delta p,\end{aligned}\tag{B5}$$

which indicates that what we perform here is a first-order *real-time* perturbation around the *quasi-equilibrium* at each moment, ensuring a comoving equilibrium distribution of ion concentration field as the two-liquid interface evolves. The zero-order equations, which only include the equilibrium terms and give the real-time quasi-equilibrium solution, are written as follows:

$$\nabla \cdot (\bar{\epsilon} \nabla \varphi^{\text{eq}}) = - \sum_i z_i e n_i^{\text{eq}},\tag{B6}$$

$$\nabla \cdot \left( (\nabla n_i^{\text{eq}} + n_i^{\text{eq}} \nabla \ln \gamma_i^\phi) - \frac{z_i e n_i^{\text{eq}}}{k_B T} \nabla \varphi^{\text{eq}} \right) = 0,\tag{B7}$$

$$0 = -\nabla p^{\text{eq}} + \mathbf{F}_e^{\text{eq}},\tag{B8}$$

with the boundary conditions at infinity

$$\varphi^{\text{eq}} = 0, \quad \nabla \varphi^{\text{eq}} = 0, \quad n_i^{\text{eq}} = n_{i,\infty}, \quad p^{\text{eq}} = 0.\tag{B9}$$

Here, the equilibrium electric force  $\mathbf{F}_e^{\text{eq}} = - \sum_i z_i e n_i^{\text{eq}} \nabla \varphi^{\text{eq}}$  is an irrotational field.

The equations containing the first-order perturbation terms are written next, in which only the linear perturbation terms are retained, and the products of the perturbation terms are ignored [105]. The governing equations become

$$\nabla \cdot (\bar{\epsilon} \nabla \delta\varphi) = - \sum_i z_i e \delta n_i,\tag{B10}$$

$$\frac{\partial \delta n_i}{\partial t} + \nabla \cdot (n_i^{\text{eq}} \delta \mathbf{u} + \delta \mathbf{J}^{**}) = 0,\tag{B11}$$

$$\nabla \cdot \delta \mathbf{u} = 0,\tag{B12}$$

$$\bar{\rho} \left( \frac{\partial \delta \mathbf{u}}{\partial t} + \delta \mathbf{u} \cdot \nabla \delta \mathbf{u} \right) = -\nabla \delta p + \nabla \cdot (\bar{\mu} \nabla \delta \mathbf{u}) + \mu_\phi \nabla \phi + \delta \mathbf{F}_e.\tag{B13}$$

Here, the linear perturbations of number flux of ion  $i$  and electric force are

$$\delta \mathbf{J}^{**} = -\bar{D}_i (\nabla \delta n_i + \delta n_i \nabla \ln \gamma_i^\phi) - \frac{z_i e \bar{D}_i}{k_B T} (\delta n_i \nabla \varphi^{\text{eq}} + n_i^{\text{eq}} \nabla \delta \varphi),\tag{B14}$$

and

$$\delta \mathbf{F}_e = - \sum_i z_i e (\delta n_i \nabla \varphi^{\text{eq}} + n_i^{\text{eq}} \nabla \delta \varphi) - \frac{1}{2} E^2 \nabla \bar{\epsilon},\tag{B15}$$

respectively. The corresponding boundary conditions at infinity are

$$\delta \varphi = 0, \quad \nabla \delta \varphi = \mathbf{E}_\infty, \quad \delta n_i = 0,$$

$$\delta \boldsymbol{\sigma} \cdot \mathbf{n} \equiv [-\delta p \mathbf{I} + \bar{\mu} (\nabla \delta \mathbf{u} + (\nabla \delta \mathbf{u})^T)] \cdot \mathbf{n} = 0.\tag{B16}$$

Note that the decomposition above cannot survive for the cases of strong nonequilibrium transport, for which a kinetic source term instead of an effective thermodynamic potential profile term in the Nernst-Planck equation instead of the modified Poisson-Boltzmann equation (6) is required.

To obtain the solution to the order of linear perturbation equations, we can take the advantage of the numerical simulation technique. At every time step, we first solve the modified Poisson-Boltzmann equation [Eqs. (B6) and (B7)] and the perturbation equations of electric potential [Eq. (B10)] and ion concentration [Eq. (B11)] for the equilibrium distribution and linear perturbation of electric potential, respectively. Then, the recombined Navier-Stokes equations from Eqs. (B8), (B12), and (B13) are solved directly in their original forms with the interface tension and the total electric force. Note that to simplify the solution process for the linear perturbation of electric potential, it is required to make some approximation to avoid solving the modified Nernst-Planck equation which is rather complicated and may be unnecessary for the near-equilibrium transport. As mentioned in Sec. I, we ignore the charge relaxation effect and thus set  $\delta n_i$  and  $\delta \mathbf{u}$  in Eqs. (B10) and (B11) to zero. However, we will obtain the following two different sets of equations:

$$\nabla \cdot (\bar{\epsilon} \nabla \delta \varphi) = 0, \quad (\text{B17})$$

$$\nabla \cdot (\bar{D}_i n_i^{\text{eq}} \nabla \delta \varphi) = 0, \quad (\text{B18})$$

For convenience, we call the first equation (B17) the *permittivity*-based equation, and the others will yield

$$\nabla \cdot (\bar{\sigma}_c \nabla \delta \varphi) = 0, \quad (\text{B19})$$

which we call the *conductivity*-based equation. Here,  $\bar{\sigma}_c = (e^2/k_B T) \sum_i z_i^2 \bar{D}_i \bar{n}_{i,\infty}^{\text{eq}}$  is simply taken as the artificial phase interpolation of electrical conductivity  $\rho_c$ , where

$$\begin{aligned} \bar{D}_i &\equiv D_i(\phi) = \sum_{\alpha} D_{i,\alpha} \phi_{\alpha}, \\ \bar{n}_{i,\infty}^{\text{eq}} &\equiv n_{i,\infty}^{\text{eq}}(\phi) = \sum_{\alpha} n_{i,\infty}^{(\alpha)} \phi_{\alpha}, \end{aligned} \quad (\text{B20})$$

which indicates that the surface conduction effect is neglected in this work. Note that if  $n_i^{\text{eq}}$  is taken as the real ionic distribution (rather than the phase interpolation here) in the unperturbed equilibrium, it can reflect the surface conduction effect *around and within* the two-liquid interface when approach (B) for free energy parameter determination is used. Here the Stokes-Einstein relation is assumed to stand across the diffuse two-liquid interface in the limit of a dilute solution to calculate the molecular diffusivity in the organic liquid phase

$$\frac{D_{i,o}}{D_{i,w}} = \frac{r_{i,w} \mu_w}{r_{i,o} \mu_o}, \quad (\text{B21})$$

in which  $r_{i,\alpha}$  represents the effective radius of ion  $i$  in solvent  $\alpha$ .

Since, in general, the three material properties are nonuniform and not linear to each other, the above two types of equations may yield inconsistent solutions in the general cases of inhomogeneous multi-physical systems. In fact, the choice of the above equations is related to the polarizability assumptions on the liquid-liquid interface for certain ion as well as on the two bulk liquid phases. Let us take the simple ions as examples. For polar organic liquid where the two-liquid partition coefficient is relatively low and the interface can be considered to be partially nonpolarizable, it is recommended to utilize the conductivity equation (B19) to achieve a good agreement with the solution recovering diffusive relaxation but still neglecting convective relaxation from our practical experience. However, for nonpolar organic liquid where the two-liquid partition coefficient is extremely low and the interface is nearly polarizable and blocking, the permittivity equation (B17) is more appropriate in terms of both the physical significance and numerical stability. The discussions for the organic ions are similar to the above. In this work, we will calculate the

linear perturbation of electric potential through either the *conductivity*-based Laplace equation with nonuniform property [Eq. (B19)] or the *permittivity*-based Laplace equation with nonuniform property [Eq. (B17)], because of the absence of the above inconsistency in the case of two-liquid parallel electroosmosis.

### APPENDIX C: THEORETICAL SOLUTION TO SHARP INTERFACE MODEL WITH GENERAL CHARGING MECHANISM

The theoretical solution to the sharp interface model will be utilized as the verification and illustration of our diffuse interface models. As a comparison, the theoretical solution to the sharp interface model of two-liquid parallel electroosmosis with a general charging mechanism will be given, where the electric potential is written in a dimensionless and displaced form  $\tilde{\varphi}/\zeta_T \equiv (\varphi - \Delta_w^0 \varphi_\infty)/\zeta_T$ , while the velocity profile is written in the dimensionless form  $U \equiv \rho_w u d_{\text{tot}}/\mu_w$ .

We start by writing the Poisson equation of the electric potential,

$$\varepsilon_\alpha \frac{\partial^2 \varphi_\alpha}{\partial y^2} = -\rho_{e,\alpha}, \quad (\text{C1})$$

with the boundary conditions at the charged solid walls,

$$(\varphi_1 - \varphi_\infty^{(1)})|_{y=d_1} = \zeta_{\text{sl}}^{(1)}, \quad (\varphi_2 - \varphi_\infty^{(2)})|_{y=-d_2} = \zeta_{\text{sl}}^{(2)}, \quad (\text{C2})$$

and the interfacial conditions at the two-liquid interface,

$$(\varphi_1 - \varphi_2)|_{y=0} =: -\Delta_1^2 \varphi_{\text{in}}, \quad \left( \varepsilon_1 \frac{\partial \varphi_1}{\partial y} - \varepsilon_2 \frac{\partial \varphi_2}{\partial y} \right) \Big|_{y=0} = -\sigma_{\text{II}}. \quad (\text{C3})$$

Note that the sharp interface model is used here and the effect of continuous variation of permittivity within the solvent mixing layer is ignored, which results in the discontinuity of the material properties and electric potential at the interface  $y = 0$ . The different phases with different bulk material properties and physical field quantities are denoted by  $\alpha (= 1, 2)$  for water and organic liquid, respectively, and  $\varphi_\infty^{(\alpha)}$  is then defined as the electrically neutral region in contact with the phase  $\alpha$ . Besides, all the possible charging mechanisms are included here phenomenologically, compared with previous studies where only the latter two are considered [35]. To be specific,  $\Delta_1^2 \varphi_\infty = \varphi_\infty^{(2)} - \varphi_\infty^{(1)}$  is induced by the imbalanced partition,  $\sigma_{\text{II}}$  is induced by the specific adsorption, while  $\Delta_1^2 \varphi_{\text{in}}$  is the effective potential jump across the solvent mixing layer. These three parameters are considered as independent ones, although  $\Delta_1^2 \varphi_{\text{in}}$  indeed originates from the capacity of solvent mixing layer and thus should be dependent on the total potential jump  $\Delta_1^2 \varphi_\infty$  as well as the surface charge density  $\sigma_{\text{II}}$  of specifically absorbed ions at interface. The following solutions derived from the sharp interface model are utilized for the quantitative verification and illuminating analysis of the results from diffuse interface model, in which the solvent mixing layer potential jump can be naturally captured.

Choosing  $\varphi_\infty^{(1)}$  as the reference point of electric potential and setting  $\tilde{\varphi}_1 = \varphi_1$  and  $\tilde{\varphi}_2 = \varphi_2 - \Delta_1^2 \varphi_\infty$ , the equilibrium ionic concentration based on the Boltzmann distribution is written as

$$\rho_{e,\alpha} = \sum_i z_i e n_i^{(\alpha)} = \sum_i z_i e n_{i,\infty}^{(\alpha)} \exp\left(-\frac{z_i e \tilde{\varphi}_\alpha}{k_B T}\right). \quad (\text{C4})$$

Using Debye-Hückel approximation under  $\max\{|\zeta_{\text{sl}}^{(\alpha)}|, |\Delta_1^2 \varphi_\infty|, |\sigma_{\text{II}} \lambda_{\text{D},\alpha}/\varepsilon_\alpha|\} \ll \zeta_T \equiv k_B T/e$ , we obtain the linearized Poisson-Boltzmann equation,

$$\lambda_{\text{D},\alpha}^2 \frac{\partial^2 \tilde{\varphi}_\alpha}{\partial y^2} = \tilde{\varphi}_\alpha, \quad (\text{C5})$$

with the Debye lengths  $\lambda_{D,\alpha} = [e^2 \sum_i z_i^2 n_{i,\infty}^{(\alpha)} / (\varepsilon_\alpha k_B T)]^{-1/2}$  in phase  $\alpha$  containing solute ions  $i$ 's. The corresponding boundary and interfacial conditions are written as

$$\tilde{\varphi}_1|_{y=d_1} = \zeta_{sl}^{(1)}, \quad \tilde{\varphi}_2|_{y=-d_2} = \zeta_{sl}^{(2)}, \quad (C6)$$

and

$$\begin{aligned} (\tilde{\varphi}_1 - \tilde{\varphi}_2)|_{y=0} &= \Delta_1^2 \varphi_\infty - \Delta_1^2 \varphi_{in}, \\ \left( \varepsilon_1 \frac{\partial \tilde{\varphi}_1}{\partial y} - \varepsilon_2 \frac{\partial \tilde{\varphi}_2}{\partial y} \right) \Big|_{y=0} &= -\sigma_{11}. \end{aligned} \quad (C7)$$

The Stokes equation of the velocity field is written as

$$0 = \mu_\alpha \frac{\partial^2 u_\alpha}{\partial y^2} + \rho_{e,\alpha} E, \quad (C8)$$

with the boundary conditions at the charged solid walls,

$$u_1|_{y=d_1} = 0, \quad u_2|_{y=-d_2} = 0, \quad (C9)$$

and the interfacial conditions at the two-liquid interface,

$$(u_1 - u_2)|_{y=0} = 0, \quad \left( \mu_1 \frac{\partial u_1}{\partial y} - \mu_2 \frac{\partial u_2}{\partial y} \right) \Big|_{y=0} = -\sigma_{11} E. \quad (C10)$$

To solve the equations, we first do the nondimensionalization,

$$\begin{aligned} y_\alpha &= y/d_\alpha, \quad H_\alpha = d_\alpha/\lambda_{D,\alpha}, \\ \Phi_\alpha &= \tilde{\varphi}_\alpha/\zeta_T, \quad U_\alpha = u_\alpha(d_1 + d_2)/v_1. \end{aligned} \quad (C11)$$

Then, the solution could be written as

$$\begin{aligned} \Phi_1 &= f_1 \frac{\cosh y_1 H_1}{\cosh H_1} + (Z_1 - f_1) \frac{\sinh y_1 H_1}{\sinh H_1}, \\ \Phi_2 &= f_2 \frac{\cosh y_2 H_2}{\cosh H_2} - (Z_2 - f_2) \frac{\sinh y_2 H_2}{\sinh H_2}, \end{aligned} \quad (C12)$$

and

$$\begin{aligned} U_1 &= U_{EO,1}^{(1)}(\Phi_1 - Z_1) - \frac{\mathcal{X}U_s}{1 + \mathcal{X}}(1 - y_1), \\ U_2 &= U_{EO,1}^{(2)}(\Phi_2 - Z_2) + \frac{U_s}{1 + \mathcal{X}}(1 + y_2), \end{aligned} \quad (C13)$$

where

$$\begin{aligned} f_1 &= \frac{Z_1 + \mathcal{B}Z_2/\mathcal{A}}{1 + \mathcal{B}} + \left( \frac{Q_s + \mathcal{B}Z_d}{1 + \mathcal{B}} \right) \cosh H_1, \\ f_2 &= \frac{\mathcal{B}Z_2 + \mathcal{A}Z_1}{1 + \mathcal{B}} + \left( \frac{Q_s - Z_d}{1 + \mathcal{B}} \right) \cosh H_2, \end{aligned} \quad (C14)$$

and

$$\begin{aligned} U_{EO,\beta}^{(\alpha)} &= \frac{U_{EO}^{(\alpha)}(d_1 + d_2)}{v_\beta}, \quad U_{EO}^{(\alpha)} = \frac{\varepsilon_\alpha \zeta_T E}{\mu_\alpha}, \\ U_s &= U_{EO,1}^{(1)}(\Phi_1(0) - Z_1) - U_{EO,1}^{(2)}(\Phi_2(0) - Z_2). \end{aligned} \quad (C15)$$

Here, the definitions of those parameters are listed below:

$$\begin{aligned} Z_\alpha &= \frac{\zeta_{sl}^{(\alpha)}}{\zeta_T}, & Q_s &= \frac{\sigma_{ll}/\zeta_T}{(\varepsilon_1/\lambda_{D,1}) \coth H_1}, & Z_d &= \frac{\Delta_1^2 \varphi_\infty - \Delta_1^2 \varphi_{in}}{\zeta_T}, \\ \mathcal{A} &= \frac{\cosh H_2}{\cosh H_1}, & \mathcal{B} &= \frac{(\varepsilon_2/\lambda_{D,2}) \coth H_2}{(\varepsilon_1/\lambda_{D,1}) \coth H_1}, & \mathcal{X} &= \frac{\mu_2/d_2}{\mu_1/d_1}. \end{aligned} \quad (C16)$$

As seen above,  $Q_s, Z_d$  are the dimensionless interfacial charge and effective potential jump at the two-liquid interface, while  $\mathcal{A}, \mathcal{B}, \mathcal{X}$  could be recognized as the effective ratios of geometric dimension, diffuse layer capacity, and dynamic viscosity, respectively. It should be noted that similar results have been derived in some previous studies, which, however, may fail to acknowledge the full applicability and physical meaning of those results.

From the above results, it is straightforward to get the surface charge at the solid walls as follows:

$$\sigma_{sl}^{(\alpha)} = \frac{\varepsilon_\alpha \zeta_T}{\lambda_{D,\alpha}} [f_\alpha \tanh H_\alpha + (Z_\alpha - f_\alpha) \coth H_\alpha] \equiv \frac{\varepsilon_\alpha \zeta_T}{\lambda_{D,\alpha}} Q_\alpha. \quad (C17)$$

After a straightforward algebraic calculation, we can express the results electric potential and velocity profiles  $\Phi_\alpha$  and  $U_\alpha$  using  $Q_\alpha$  as follows:

$$f_\alpha = \frac{Q_\alpha - Z_\alpha \coth H_\alpha}{\tanh H_\alpha - \coth H_\alpha}. \quad (C18)$$

Then the result can be obtained through linear transformations  $(Z_1, Z_2) = \mathbf{Z}(Q_1, Q_2)$  and  $(f_1, f_2) = \mathbf{f}(Q_1, Q_2)$ , which we neglect the details here.

#### APPENDIX D: ESTIMATION OF PROPERTIES OF TWO-LIQUID SYSTEM WITH MULTIPLE ELECTROLYTES

Following the choice in Sec. III B, we choose *n*-decane and nitrobenzene to capture the characteristics of nonpolar and polar organic liquids, and the constituent ions include  $\text{H}^+$ ,  $\text{OH}^-$ , and  $\text{Ph}_4\text{As}^+$  as the adsorption-induced potential-determining and impurity ions, respectively, as well as  $\text{K}^+$ ,  $\text{Cl}^-$  as the support electrolyte.

The material properties of the water and organic liquid phases take the values of

$$\begin{aligned} \varepsilon_w &= 80\varepsilon_0, & \mu_w &= 1.00 \text{ mPa s}, & \rho_w &= 1.0 \times 10^3 \text{ kg/m}^3, \\ \varepsilon_o^{(\text{np})} &= 2\varepsilon_0, & \mu_o^{(\text{np})} &= 0.85 \text{ mPa s}, & \rho_o^{(\text{np})} &= 0.73 \times 10^3 \text{ kg/m}^3, \\ \varepsilon_o^{(\text{p})} &= 35\varepsilon_0, & \mu_o^{(\text{p})} &= 1.86 \text{ mPa s}, & \rho_o^{(\text{p})} &= 1.2 \times 10^3 \text{ kg/m}^3. \end{aligned}$$

The hydrated radii and bare radii of the ions in water phase are taken as [106,107]

$$\begin{aligned} r_{\text{H}_3\text{O}^+, \text{hydra}} &= 0.28 \text{ nm}, & r_{\text{H}^+, \text{bare}} &= 0.112 \text{ nm}, \\ r_{\text{OH}^-, \text{hydra}} &= 0.30 \text{ nm}, & r_{\text{OH}^-, \text{bare}} &= 0.176 \text{ nm}, \\ r_{\text{K}^+, \text{hydra}} &= 0.33 \text{ nm}, & r_{\text{K}^+, \text{bare}} &= 0.133 \text{ nm}, \\ r_{\text{Cl}^-, \text{hydra}} &= 0.33 \text{ nm}, & r_{\text{Cl}^-, \text{bare}} &= 0.181 \text{ nm}, \\ r_{\text{Ph}_4\text{As}^+, \text{hydra}} &\simeq r_{\text{Ph}_4\text{As}^+, \text{bare}} = 0.428 \text{ nm}. \end{aligned}$$

The molecular diffusivities of ions in water phase are set to [108]

$$\begin{aligned} D_{\text{H}^+, \text{w}} &= 9.312 \times 10^{-9} \text{ m}^2/\text{s}, & D_{\text{OH}^-, \text{w}} &= 5.260 \times 10^{-9} \text{ m}^2/\text{s}, \\ D_{\text{K}^+, \text{w}} &= 1.957 \times 10^{-9} \text{ m}^2/\text{s}, & D_{\text{Cl}^-, \text{w}} &= 2.032 \times 10^{-9} \text{ m}^2/\text{s}, \\ D_{\text{Ph}_4\text{As}^+, \text{w}} &\simeq 0.85 \times 10^{-9} \text{ m}^2/\text{s}. \end{aligned}$$

Here, with regard to the unknown properties of  $\text{Ph}_4\text{As}^+$ , its hydrated radius is taken as the same value as the bare one considering the large nonpolar benzene shell encircles the central metal ion [106], and its molecular diffusivity is taken as the value of  $\text{Pt}_4\text{N}^+$  whose ion radius is similar [107].

The free energies of adsorption for both the nonpolar and polar organic liquids with inert surfaces are valued at  $\mathcal{G}_{\text{a,OH}^-}^{(\text{exp})} = -25$  and  $\mathcal{G}_{\text{a,others}}^{(\text{exp})} \simeq 0$  according to the previous experiments. As for the free energies of transfer, the following results are obtained from experiments for the polar organic liquid [32,109]

$$\mathcal{G}_{\text{t,Ph}_4\text{As}^+}^{(\text{p,exp})} = (-14.3 \pm 0.2), \quad \mathcal{G}_{\text{t,K}^+}^{(\text{p,exp})} = (9.2 \pm 0.6), \quad \mathcal{G}_{\text{t,Cl}^-}^{(\text{p,exp})} = (13.2 \pm 0.9),$$

while few experimental results are available for other necessary data and theoretical evaluation is required. If using the Born potential model as follows:

$$\Delta_{\beta}^{\alpha} g_{\text{t},i}^0(\text{Born}) = \frac{z_i^2 e^2}{2\epsilon_0 r_{i,\text{bare}}} \left( \frac{1}{\epsilon_{\alpha}} - \frac{1}{\epsilon_{\beta}} \right), \quad (\text{D1})$$

where  $r_{i,\text{bare}}$  is the bare radius of ion  $i$  and  $\epsilon_{\alpha(\beta)} \equiv \epsilon_{\alpha(\beta),0}$  are the low-frequency relative permittivities of phase  $\alpha(\beta)$ , respectively, we obtain

$$\mathcal{G}_{\text{t,Ph}_4\text{As}^+}^{(\text{p,Born})} = 13.2, \quad \mathcal{G}_{\text{t,K}^+}^{(\text{p,Born})} = 42.5, \quad \mathcal{G}_{\text{t,Cl}^-}^{(\text{p,Born})} = 31.2.$$

It is clearly seen that this model overestimates the free energy of transfer. Therefore, the nonlocal electrostatics method is utilized instead, which includes extra free parameter to fit the experimental results of free energy of transfer.

To be specific, the nonlocal electrostatics model is written as

$$\begin{aligned} \Delta_{\beta}^{\alpha} g_{\text{t},i}^0(\text{nonloc}) &= \Delta_{\beta}^{\alpha} g_{\text{t},i}^0(\text{el}) + \Delta_{\beta}^{\alpha} g_{\text{t},i}^0(\text{ne}) \\ &\equiv \Delta_{\text{vac}}^{\alpha} g_{\text{t},i}^0(\text{el}) - \Delta_{\text{vac}}^{\beta} g_{\text{t},i}^0(\text{el}) + \Delta_{\beta}^{\alpha} g_{\text{t},i}^0(\text{ne}), \end{aligned} \quad (\text{D2})$$

where the electrostatic part is derived using a nonlocal electrostatics method

$$\Delta_{\text{vac}}^{\alpha} g_{\text{t},i}^0(\text{el}) = -\frac{z_i^2 e^2}{2\epsilon_0 r_i} \left[ 1 - \frac{1}{\epsilon_{\alpha_1}} + \left( \frac{1}{\epsilon_{\alpha_1}} - \frac{1}{\epsilon_{\alpha_2}} \right) \psi\left(\frac{2r_i}{\lambda_{\alpha_2}}\right) + \left( \frac{1}{\epsilon_{\alpha_2}} - \frac{1}{\epsilon_{\alpha_3}} \right) \psi\left(\frac{2r_i}{\lambda_{\alpha_3}}\right) \right], \quad (\text{D3})$$

and the nonelectrostatic part is represented by the semiempirical Uhlig formula

$$\Delta_{\beta}^{\alpha} g_{\text{t},i}^0(\text{ne}) = 4\pi r_i^2 \gamma_{\alpha\beta} \text{sign}(\gamma_{\alpha 0} - \gamma_{\beta 0}). \quad (\text{D4})$$

Here,  $r_i$  is the effective radius of ion  $i$ ,  $\epsilon_{\alpha_1}, \epsilon_{\alpha_2}, \epsilon_{\alpha_3}$  are the characteristic permittivities of solvent  $\alpha$ ,  $\lambda_{\alpha_2}, \lambda_{\alpha_3}$  are the correlation lengths as fitting parameters, and  $\psi(x) = 1 - (1 - e^{-x})/2$ , while  $\gamma_{\alpha\beta}$  denotes the interfacial tension at flat boundary between the solvents, and  $\gamma_{\alpha 0}(\gamma_{\beta 0})$  denote the surface tensions at the boundaries of solvents  $\alpha(\beta)$ , respectively. In this work, the permittivities and correlation lengths for water are chosen from literatures, i.e.,  $\epsilon_{\text{w},1} \equiv n_{\text{w,op}}^2 \epsilon_0 = 1.78\epsilon_0$ ,  $\epsilon_{\text{w},2} = 4.9\epsilon_0$ ,  $\epsilon_{\text{w},3} \equiv \epsilon_{\text{w},0} = 80\epsilon_0$ , and  $\lambda_{\text{w},2} = 0.1$  nm,  $\lambda_{\text{w},3} = 0.7$  nm. For polar organic liquid (nitrobenzene), given  $\epsilon_{\text{o},1}^{(\text{p})} = 2.4\epsilon_0$ ,  $\epsilon_{\text{o},2}^{(\text{p})} = 3.7\epsilon_0$ ,  $\epsilon_{\text{o},3}^{(\text{p})} = 35.0\epsilon_0$ , the correlation lengths are fitted using the experimental result for  $\text{K}^+$ ,  $\text{Cl}^-$  and  $\text{Ph}_4\text{As}^+$  through nitrobenzene-water interface as follows:

$$\lambda_{\text{o},2}^{(\text{p})} = 0.28 \text{ nm}, \quad \lambda_{\text{o},3}^{(\text{p})} = 0.40 \text{ nm},$$

which give the estimated values of

$$\mathcal{G}_{\text{t,Ph}_4\text{As}^+}^{(\text{p,nonloc})} = -16.75, \quad \mathcal{G}_{\text{t,K}^+}^{(\text{p,nonloc})} = 5.47, \quad \mathcal{G}_{\text{t,Cl}^-}^{(\text{p,nonloc})} = 18.66.$$

In particular, the radius of hydrogen ion is taken as  $r_{\text{H}_3\text{O}^+}$  in the calculation of free energy of transfer, while the bare radii are used for the other ions. For nonpolar organic liquid ( $n$ -decane), the characteristic permittivities are selected to the identical value  $\epsilon_{\text{o},1}^{(\text{np})} = \epsilon_{\text{o},2}^{(\text{np})} = \epsilon_{\text{o},3}^{(\text{np})} = 2\epsilon_0$ , while

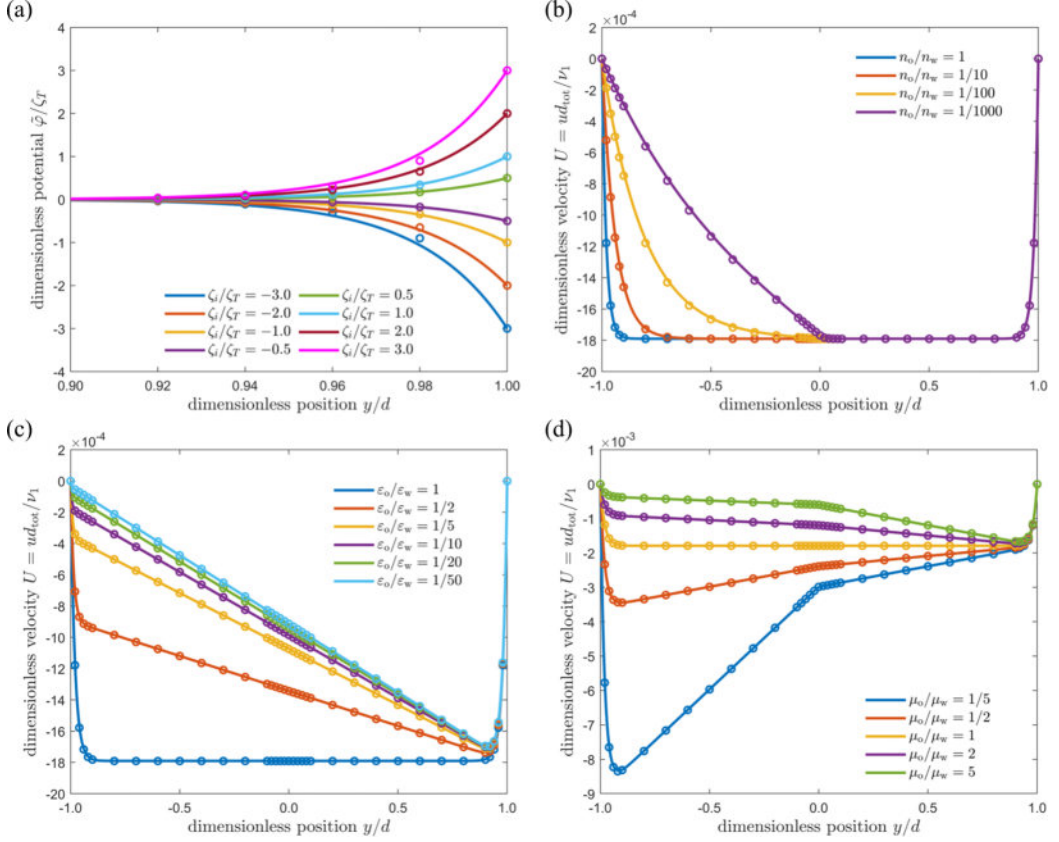


FIG. 7. Dimensionless displaced electric potential and velocity profiles when the two-liquid interface charging is absent. The circles are the simulation results of the diffuse interface model, and the lines are the theoretical solutions of the sharp interface model. As default, the material property ratios  $\varepsilon_r$ ,  $\mu_r$ ,  $\rho_r$  and the bulk ionic concentration ratio  $n_r$  are taken as 1, the  $\zeta$  potentials at solid boundaries  $\zeta_1 = \zeta_2 = \zeta_T$ .

its correlation lengths are chosen as similar values to dichloromethane due to the lacking data from experiments, i.e.,  $\lambda_{0,2}^{(\text{np})} = 0.1$  nm,  $\lambda_{0,3}^{(\text{np})} = 0.5$  nm. The free energies of transfer are then calculated as in Sec. III B and are insensitive to the correlation lengths since the permittivity of *n*-decane is quite small.

Since there are more than two types of constituent ions in the present case, Eqs. (A2) and (A3) should be extended to a more general form. This indeed has been elaborated in the previous literatures [102], and here we only briefly elucidate the procedure to determine the required distribution potential and ionic concentration ratio. Basically, there are eleven parameters to be determined including the bulk ionic concentrations  $c_{i,\alpha} \equiv c_{i,\infty}^{(\alpha)}$  ( $i = \text{H}^+, \text{OH}^-, \text{K}^+, \text{Cl}^-, \text{Ph}_4\text{As}^+$ , and  $\alpha = \text{w}, \text{o}$ ), and the distribution potential  $\Phi_\infty \equiv e\Delta_\omega^0\varphi_\infty/k_B T$ . The constraints include the electrically neutral conditions in the bulk phases,

$$\sum_i z_i c_{i,\text{w}} = 0, \quad \sum_i z_i c_{i,\text{o}} = 0, \quad (\text{D5})$$

the electrochemical potential balances for each ion  $i$ ,

$$c_{i,\text{o}} = c_{i,\text{w}} P_i \exp(-z_i \Phi_\infty), \quad (\text{D6})$$

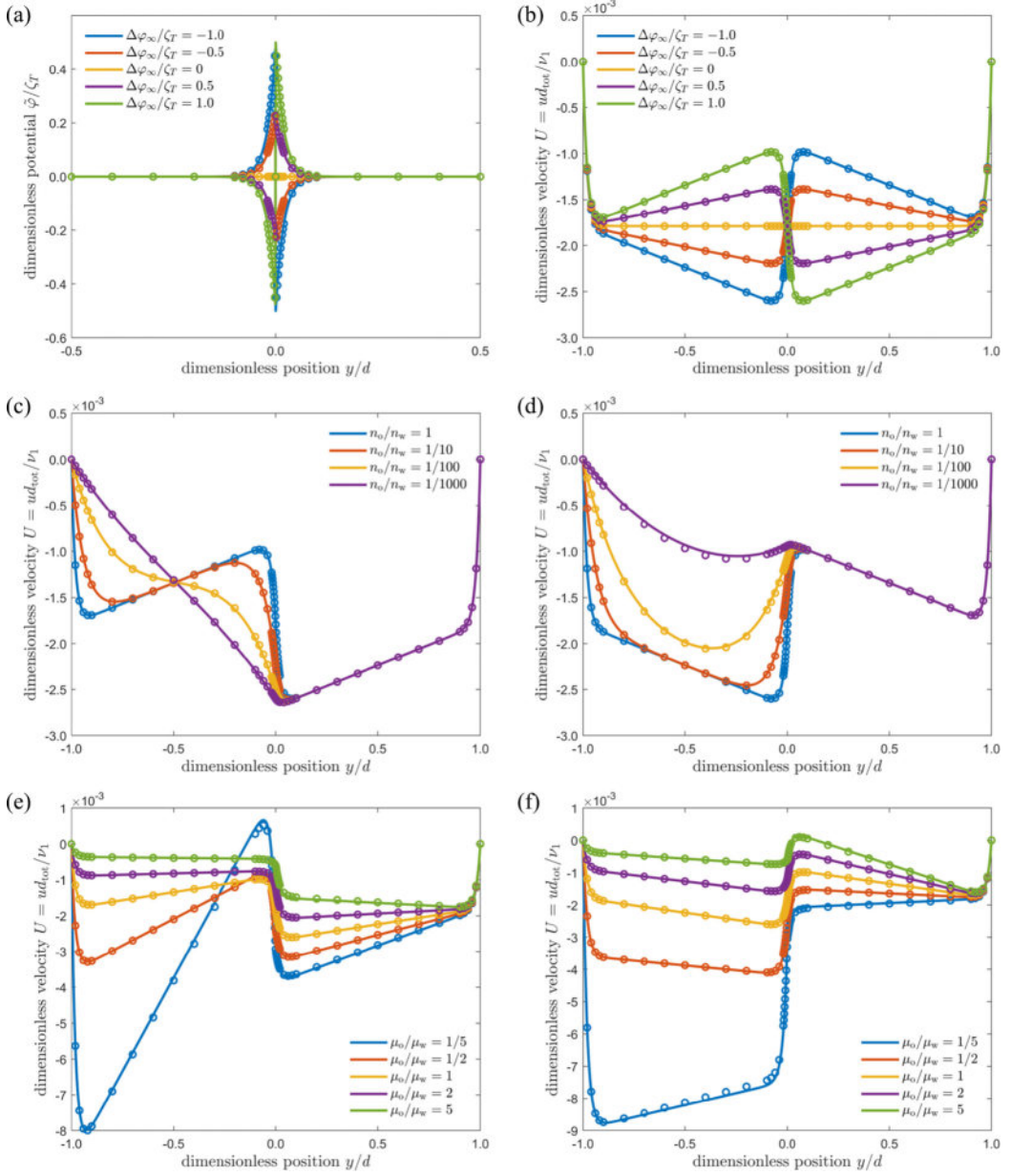


FIG. 8. Dimensionless displaced electric potential and velocity profiles when only the partition-induced two-liquid interface charging exists. The circles are the simulation results of the diffuse interface model, and the lines are the theoretical solutions of the sharp interface model. As default, the material property ratios  $\epsilon_r$ ,  $\mu_r$ ,  $\rho_r$  and the bulk ionic concentration ratio  $n_r$  are taken as 1, the  $\zeta$  potentials at solid boundaries  $\zeta_1 = \zeta_2 = \zeta_T$ . The distribution potential  $\Delta\varphi_\infty$  is set to  $\zeta_T$  for panels (c) and (e), and to  $-\zeta_T$  for panels (d) and (f).

and the dissociation equilibrium of water ions,

$$c_{\text{H}^+, \text{w}} c_{\text{OH}^-, \text{w}} = K_w. \quad (\text{D7})$$

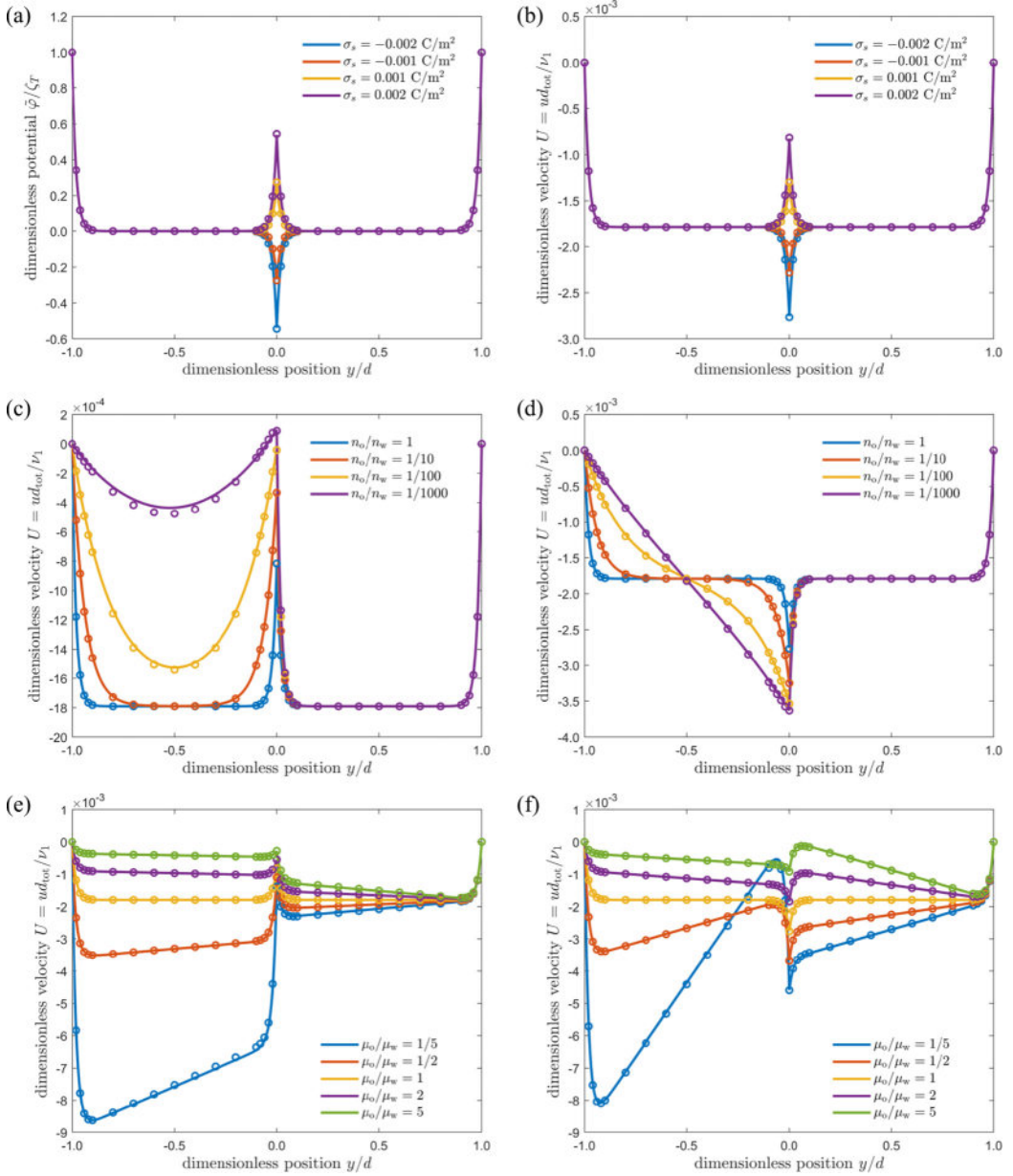


FIG. 9. Dimensionless displaced electric potential and velocity profiles when only the adsorption-induced two-liquid interface charging exists. The circles are the simulation results of the diffuse interface model, and the lines are the theoretical solutions of the sharp interface model. As default, the material property ratios  $\epsilon_r$ ,  $\mu_r$ ,  $\rho_r$  and the bulk ionic concentration ratio  $n_r$  are taken as 1, the  $\zeta$  potentials at solid boundaries  $\zeta_1 = \zeta_2 = \zeta_T$ . The interfacial charge density  $\sigma_{\text{II}}^{(w)}$  is set to  $0.002$  C/m<sup>2</sup> for panels (c) and (e), and to  $-0.002$  C/m<sup>2</sup> for panels (d) and (f).

Here,  $P_i$  represents the partition coefficient  $P_i^{o/w}$  of ion  $i$ , and  $K_w \equiv 10^{-14}$  M<sup>2</sup> is the self-ionization equilibrium constant of water. Therefore, there are three independent parameters and here we choose pH,  $c_{\text{Cl}^-,w}$ , and  $c_{\text{Ph}_4\text{As}^+,w(o)}$  for the potential-determining ion  $\text{OH}^-$ , support electrolyte KCl, and

impurity ion  $\text{Ph}_4\text{As}^+$ , respectively. Given these three parameters, the distribution potential  $\Phi_\infty$  and total ionic concentration (ionic strength) ratio  $n_r \equiv I_r := \sum_i z_i^2 c_{i,o} / \sum_i z_i^2 c_{i,w}$  are then obtained after solving these eight constraint equations for the other eight unknown parameters.

#### APPENDIX E: VERIFICATION OF NUMERICAL METHOD BASED ON DIFFUSE INTERFACE MODEL

The system setup is essentially the same as Sec. III A 1. Figure 7 depicts the results when the interface charging at the two-liquid interface is absent. It is shown that the simulation results are in great quantitative agreement with the theoretical solution, except the ones for  $|\zeta_i/\zeta_T| > 1$  in Fig. 7(a) in which the linearized theoretical solution deviates from the accurate result obtained from the diffuse interface model since the Debye-Hückel approximation becomes invalid. The results in Figs. 7(b)–7(d) illustrate that even the two-liquid interface is not spontaneously charged, its electrokinetic behavior can still be regulated by tuning the material properties of the liquid phases and is completely different from the classical solid-water ones due to the possible ion partitioning, finite solvent permittivity ratio, and finite dynamic viscosity ratio between the organic liquid and water phases. This has been elaborated in previous literatures on the two-liquid streaming potential effects triggered by the uncharged drop inside the capillary [110–112].

Effects of imbalanced ion partition and specific ion adsorption on the two-liquid parallel electroosmosis are shown in Figs. 8 and 9, respectively. It is seen that the two different charging mechanisms lead to velocity profiles with different symmetries when all the material properties and ionic concentration ratio are matched, as shown in Figs. 8(a) and 8(b) and Figs. 9(a) and 9(b). In particular, when the permittivity ratio is equal to 1, the simulation results are in great quantitative agreement with the theoretical solution, except the ones for large ionic concentration ratio  $n_r$  shown in Figs. 8(d) and 9(c) and small dynamic viscosity ratio  $\mu_r$  shown in Figs. 8(e) and 8(f) and Figs. 9(e) and 9(f). With regard to the former, the discrepant results from the strong overlapping and interaction between the electrical double layers at the solid-organic liquid and two-liquid interface. This intensively amplifies the errors induced by the electric potential interfacial conditions in the sharp interface model at the two-liquid interface. As for the latter, the inconsistency lies in the large shear rate at the two-liquid interface when the dynamic viscosity of organic liquid phase goes down and its continuous transition across the interface with the linear interpolation function of  $\mu(\phi)$  may extend to a finite distance which is comparable to the thickness of the diffuse layer. This will result in the remarkable derivations of the stress-matching interfacial condition in the sharp interface model from the diffuse interface results at the two-liquid interface. The above deviations show the necessity of diffuse interface model when dealing with the electrokinetic multiphase flow systems in which a rather precise description on the two-liquid interfacial dynamics is required for the large field gradient and strong coupling behaviors caused by the two-liquid interfacial charging and electrical double layer formation. In this simplest example of two-liquid parallel electroosmosis, it is indicated that for polar organic liquid whose permittivity is close to the water or of relatively low viscosity, it is mandatory to use diffuse interface models for the two-liquid electrokinetic problem of charged organic liquid droplets at the micrometer scale if an accurate prediction of interfacial stress and velocity profile is needed.

- 
- [1] J. Israelachvili and H. Wennerström, Role of hydration and water structure in biological and colloidal interactions, *Nature (London)* **379**, 219 (1996).
  - [2] D. Chandler, Interfaces and the driving force of hydrophobic assembly, *Nature (London)* **437**, 640 (2005).
  - [3] E. E. Meyer, K. J. Rosenberg, and J. Israelachvili, Recent progress in understanding hydrophobic interactions, *Proc. Natl. Acad. Sci. USA* **103**, 15739 (2006).

- [4] G. Luo, S. Malkova, J. Yoon, G. Schultz David, B. Lin, M. Meron, I. Benjamin, P. Vanýsek, and M. L. Schlossman, Ion distributions near a liquid-liquid interface, *Science* **311**, 216 (2006).
- [5] N. Laanait, M. Mihaylov, B. Hou, H. Yu, P. Vanýsek, M. Meron, B. Lin, I. Benjamin, and M. L. Schlossman, Tuning ion correlations at an electrified soft interface, *Proc. Natl. Acad. Sci. USA* **109**, 20326 (2012).
- [6] P. Li, J. Liu, J.-H. Yuan, Y. Guo, S. Wang, P. Zhang, and W. Wang, Artificial funnel nanochannel device emulates synaptic behavior, *Nano Lett.*, **24**, 6192 (2024).
- [7] A. Maurice, J. Theisen, and J.-C. P. Gabriel, Microfluidic lab-on-chip advances for liquid-liquid extraction process studies, *Curr. Opin. Colloid Interface Sci.* **46**, 20 (2020).
- [8] B. Schuur, T. Brouwer, and L. M. J. Sprakel, Recent developments in solvent-based fluid separations, *Annu. Rev. Chem. Biomol. Eng.* **12**, 573 (2021).
- [9] Y. Chao, O. Ramírez-Soto, C. Bahr, and S. Karpitschka, How liquid-liquid phase separation induces active spreading, *Proc. Natl. Acad. Sci. USA* **119**, e2203510119 (2022).
- [10] J. T. Tetteh, P. V. Brady, and R. Barati Ghahfarokhi, Review of low salinity waterflooding in carbonate rocks: Mechanisms, investigation techniques, and future directions, *Adv. Colloid Interface Sci.* **284**, 102253 (2020).
- [11] H. Tian and M. Wang, Electrokinetic mechanism of wettability alternation at oil-water-rock interface, *Surf. Sci. Rep.* **72**, 369 (2017).
- [12] F. Liu and M. Wang, Review of low salinity waterflooding mechanisms: Wettability alteration and its impact on oil recovery, *Fuel* **267**, 117112 (2020).
- [13] M. Li and D. Li, Bidirectional transfer of particles across liquid-liquid interface under electric pulse, *J. Colloid Interface Sci.* **560**, 436 (2020).
- [14] Y. Chao and H. C. Shum, Emerging aqueous two-phase systems: From fundamentals of interfaces to biomedical applications, *Chem. Soc. Rev.* **49**, 114 (2020).
- [15] Y. Lu, L. Jiang, Y. Yu, D. Wang, W. Sun, Y. Liu, J. Yu, J. Zhang, K. Wang, H. Hu, X. Wang, Q. Ma, and X. Wang, Liquid-liquid triboelectric nanogenerator based on the immiscible interface of an aqueous two-phase system, *Nat. Commun.* **13**, 5316 (2022).
- [16] A. Brask, G. Goranović, M. J. Jensen, and H. Bruus, A novel electro-osmotic pump design for nonconducting liquids: Theoretical analysis of flow rate-pressure characteristics and stability, *J. Micromech. Microeng.* **15**, 883 (2005).
- [17] Z. Ding, Y. Jian, and W. Tan, Electrokinetic energy conversion of two-layer fluids through nanofluidic channels, *J. Fluid Mech.* **863**, 1062 (2019).
- [18] A. Alizadeh, Y. Huang, F. Liu, H. Daiguji, and M. Wang, A streaming-potential-based microfluidic measurement of surface charge at immiscible liquid-liquid interface, *Int. J. Mech. Sci.* **247**, 108200 (2023).
- [19] T. M. Squires, Electrokinetic flows over inhomogeneously slipping surfaces, *Phys. Fluids* **20**, 092105 (2008).
- [20] B. Fan, A. Bhattacharya, and P. R. Bandaru, Enhanced voltage generation through electrolyte flow on liquid-filled surfaces, *Nat. Commun.* **9**, 4050 (2018).
- [21] R. J. Hunter, Recent developments in the electroacoustic characterisation of colloidal suspensions and emulsions, *Colloids Surf., A* **141**, 37 (1998).
- [22] K. G. Marinova, R. G. Alargova, N. D. Denkov, O. D. Velev, D. N. Petsev, I. B. Ivanov, and R. P. Borwankar, Charging of oil-water interfaces due to spontaneous adsorption of hydroxyl ions, *Langmuir* **12**, 2045 (1996).
- [23] S. S. Dukhin, Non-equilibrium electric surface phenomena, *Adv. Colloid Interface Sci.* **44**, 1 (1993).
- [24] F. Yang, S. Shin, and H. A. Stone, Diffusiophoresis of a charged drop, *J. Fluid Mech.* **852**, 37 (2018).
- [25] F. Liu and M. Wang, Wettability effects on mobilization of ganglia during displacement, *Int. J. Mech. Sci.* **215**, 106933 (2022).
- [26] A. J. Pascall and T. M. Squires, Electrokinetics at liquid/liquid interfaces, *J. Fluid Mech.* **684**, 163 (2011).
- [27] P. Vanýsek, *Electrochemistry on Liquid/Liquid Interfaces*, 1st ed., Lecture Notes in Chemistry (Springer, Berlin, Heidelberg, 1985), pp. 3–51.

- [28] A. G. Volkov, D. W. Deamer, D. L. Tanelian, and V. S. Markin, Electrical double layers at the oil/water interface, *Prog. Surf. Sci.* **53**, 1 (1996).
- [29] A. G. Volkov and V. S. Markin, Chapter 4 electric properties of oil/water interfaces, in *Interface Science and Technology* (Elsevier, Amsterdam, 2004), Vol. 4, pp. 91–182.
- [30] Y. Marcus, Single ion Gibbs free energies of transfer from water to organic and mixed solvents, *Rev. Anal. Chem.* **5**, 53 (1980).
- [31] Y. Marcus, Thermodynamic functions of transfer of single ions from water to nonaqueous and mixed solvents: Part I - Gibbs free energies of transfer to nonaqueous solvents, *Pure Appl. Chem.* **55**, 977 (1983).
- [32] V. S. Markin and A. G. Volkov, The Gibbs free energy of ion transfer between two immiscible liquids, *Electrochim. Acta* **34**, 93 (1989).
- [33] A. G. Volkov and D. W. Deamer, Redox chemistry at liquid-liquid interfaces, in *Progress in Colloid and Polymer Science* (Steinkopff, 1997), Vol. 103, pp. 21–28.
- [34] Z. Samec, Electrical double layer at the interface between two immiscible electrolyte solutions, *Chem. Rev.* **88**, 617 (1988).
- [35] W. Choi, A. Sharma, S. Qian, G. Lim, and S. W. Joo, On steady two-fluid electroosmotic flow with full interfacial electrostatics, *J. Colloid Interface Sci.* **357**, 521 (2011).
- [36] O. Schnitzer and E. Yariv, The Taylor–Melcher leaky dielectric model as a macroscale electrokinetic description, *J. Fluid Mech.* **773**, 1 (2015).
- [37] Y. Mori and Y. N. Young, From electrodiffusion theory to the electrohydrodynamics of leaky dielectrics through the weak electrolyte limit, *J. Fluid Mech.* **855**, 67 (2018).
- [38] Y. Uematsu and H. Ohshima, Electrophoretic mobility of a water-in-oil droplet separately affected by the net charge and surface charge density, *Langmuir* **38**, 4213 (2022).
- [39] F. Booth, The cataphoresis of spherical fluid droplets in electrolytes, *J. Chem. Phys.* **19**, 1331 (1951).
- [40] J. C. Baygents and D. Saville, Electrophoresis of drops and bubbles, *J. Chem. Soc. Faraday Trans.* **87**, 1883 (1991).
- [41] R. Scardovelli and S. Zaleski, Direct numerical simulation of free-surface and interfacial flow, *Annu. Rev. Fluid Mech.* **31**, 567 (1999).
- [42] D. M. Anderson, G. B. McFadden, and A. A. Wheeler, Diffuse-interface methods in fluid mechanics, *Annu. Rev. Fluid Mech.* **30**, 139 (1998).
- [43] J. A. Sethian and P. Smereka, Level set methods for fluid interfaces, *Annu. Rev. Fluid Mech.* **35**, 341 (2003).
- [44] H. Davis and L. Scriven, Stress and structure in fluid interfaces, *Adv. Chem. Phys.* **49**, 357 (1982).
- [45] J. J. Feng, C. Liu, J. I. E. Shen, and P. Yue, A diffuse-interface method for simulating two-phase flows of complex fluids, *J. Fluid Mech.* **515**, 293 (2004).
- [46] R. Krishna and J. A. Wesselingh, The Maxwell-Stefan approach to mass transfer, *Chem. Eng. Sci.* **52**, 861 (1997).
- [47] M. Li and D. Li, Redistribution of mobile surface charges of an oil droplet in water in applied electric field, *Adv. Colloid Interface Sci.* **236**, 142 (2016).
- [48] Y. He, P. Yazhgor, A. Salonen, and D. Langevin, Adsorption–desorption kinetics of surfactants at liquid surfaces, *Adv. Colloid Interface Sci.* **222**, 377 (2015).
- [49] E. Kian Far, M. Gorakifard, and E. Fattahi, Multiphase phase-field lattice Boltzmann method for simulation of soluble surfactants, *Symmetry* **13**, 1019 (2021).
- [50] B. Rotenberg, I. Pagonabarraga, and D. Frenkel, Coarse-grained simulations of charge, current and flow in heterogeneous media, *Faraday Discuss.* **144**, 223 (2010).
- [51] J. J. Huang, C. Shu, J. J. Feng, and Y. T. Chew, A phase-field-based hybrid lattice-Boltzmann finite-volume method and its application to simulate droplet motion under electrowetting control, *J. Adhes. Sci. Technol.* **26**, 1825 (2012).
- [52] O. Shardt, S. K. Mitra, and J. J. Derksen, Simulations of charged droplet collisions in shear flow, *Chem. Eng. J.* **302**, 314 (2016).
- [53] N. Rivas, S. Frijters, I. Pagonabarraga, and J. Harting, Mesoscopic electrohydrodynamic simulations of binary colloidal suspensions, *J. Chem. Phys.* **148**, 144101 (2018).

- [54] R. A. W. Dryfe, The electrified liquid-liquid interface, *Adv. Chem. Phys.* **141**, 153 (2009).
- [55] T. Krüger, H. Kusumaatmaja, A. Kuzmin, O. Shardt, G. Silva, and E. M. Viggen, *The Lattice Boltzmann Method: Principles and Practice* (Springer, Berlin, 2017).
- [56] D. Jacqmin, Contact-line dynamics of a diffuse fluid interface, *J. Fluid Mech.* **402**, 57 (2000).
- [57] T. Kakiuchi, Electrochemical instability at liquid/liquid interfaces, in *Interfacial Nanochemistry* (Springer, Berlin, 2005), pp. 155–170.
- [58] A. Riaud, S. Zhao, K. Wang, Y. Cheng, and G. Luo, Lattice-Boltzmann method for the simulation of multiphase mass transfer and reaction of dilute species, *Phys. Rev. E* **89**, 053308 (2014).
- [59] Y. Uematsu, D. J. Bonthuis, and R. R. Netz, Impurity effects at hydrophobic surfaces, *Curr. Opin. Electrochem.* **13**, 166 (2019).
- [60] J. B. Sweeney, L. E. Scriven, and H. T. Davis, Gradient theory of the electric double layer at hydrocarbon–water interfaces, *J. Chem. Phys.* **87**, 6120 (1987).
- [61] K. Luo, Y. Zhang, J. Wu, H.-L. Yi, and H.-P. Tan, Lattice Boltzmann modeling of two-phase electrohydrodynamic flows under unipolar charge injection, *Phys. Rev. E* **105**, 065304 (2022).
- [62] J. M. López-Herrera, S. Popinet, and M. A. Herrada, A charge-conservative approach for simulating electrohydrodynamic two-phase flows using volume-of-fluid, *J. Comput. Phys.* **230**, 1939 (2011).
- [63] D. He and H. Huang, A contact line dynamic model for a conducting water drop on an electrowetting device, *Commun. Comput. Phys.* **20**, 811 (2016).
- [64] C. Wang, Y. Song, X. Pan, and D. Li, Translational velocity of a charged oil droplet close to a horizontal solid surface under an applied electric field, *Int. J. Heat Mass Transf.* **132**, 322 (2019).
- [65] Y. Wu, L. Fan, E. Jian, and E. Lee, Electrophoresis of a highly charged dielectric fluid droplet in electrolyte solutions, *J. Colloid Interface Sci.* **598**, 358 (2021).
- [66] C. Wang, Q. Gao, and Y. Song, Electrokinetic effect of a two-liquid interface within a slit microchannel, *Langmuir* **39**, 17529 (2023).
- [67] R. C. Tolman, Consideration of the Gibbs theory of surface tension, *J. Chem. Phys.* **16**, 758 (1948).
- [68] H. Sasaki, A. Muramatsu, H. Arakatsu, and S. Usui,  $\zeta$  potential measurement by means of the plane interface technique, *J. Colloid Interface Sci.* **142**, 266 (1991).
- [69] J. Kim, Phase-field models for multi-component fluid flows, *Commun. Comput. Phys.* **12**, 613 (2012).
- [70] Y. Q. Zu and S. He, Phase-field-based lattice Boltzmann model for incompressible binary fluid systems with density and viscosity contrasts, *Phys. Rev. E* **87**, 043301 (2013).
- [71] J. Maes and C. Soulaine, A unified single-field volume-of-fluid-based formulation for multi-component interfacial transfer with local volume changes, *J. Comput. Phys.* **402**, 109024 (2020).
- [72] T. Inamuro, T. Ogata, S. Tajima, and N. Konishi, A lattice Boltzmann method for incompressible two-phase flows with large density differences, *J. Comput. Phys.* **198**, 628 (2004).
- [73] T. Lee and C.-L. Lin, A stable discretization of the lattice Boltzmann equation for simulation of incompressible two-phase flows at high density ratio, *J. Comput. Phys.* **206**, 16 (2005).
- [74] G. Tomar, D. Gerlach, G. Biswas, N. Alleborn, A. Sharma, F. Durst, S. W. J. Welch, and A. Delgado, Two-phase electrohydrodynamic simulations using a volume-of-fluid approach, *J. Comput. Phys.* **227**, 1267 (2007).
- [75] Q. Liu, J. Zhang, and J. Wu, Direct numerical simulations of incompressible multiphase electrohydrodynamic flow with single-phase transportation schemes, [arXiv:2207.08152](https://arxiv.org/abs/2207.08152).
- [76] W. Rohlf, G. F. Dietze, H. D. Haustein, and R. Kneer, Two-phase electrohydrodynamic simulations using a volume-of-fluid approach: A comment, *J. Comput. Phys.* **231**, 4454 (2012).
- [77] Q. Yang, B. Q. Li, and Y. Ding, 3D phase field modeling of electrohydrodynamic multiphase flows, *Int. J. Multiphase Flow* **57**, 1 (2013).
- [78] E. J. W. Verwey and K. F. Niessen, XI. The electrical double layer at the interface of two liquids, *London, Edinburgh Dublin Philos. Mag. J. Sci.* **28**, 435 (1939).
- [79] L. Zhang and M. Wang, Modeling of electrokinetic reactive transport in micropore using a coupled lattice Boltzmann method, *J. Geophys. Res.: Solid Earth* **120**, 2877 (2015).
- [80] M. O. Abu-Al-Saud, S. Esmailzadeh, A. Riaz, and H. A. Tchelepi, Pore-scale study of water salinity effect on thin-film stability for a moving oil droplet, *J. Colloid Interface Sci.* **569**, 366 (2020).

- [81] A. Donev, A. L. Garcia, J.-P. Péraud, A. J. Nonaka, and J. B. Bell, Fluctuating hydrodynamics and Debye-Hückel-Onsager theory for electrolytes, *Curr. Opin. Electrochem.* **13**, 1 (2019).
- [82] M. Mirzadeh and M. Z. Bazant, Electrokinetic control of viscous fingering, *Phys. Rev. Lett.* **119**, 174501 (2017).
- [83] Y. Ma, M. Sun, X. Duan, A. van den Berg, J. C. T. Eijkel, and Y. Xie, Dimension-reconfigurable bubble film nanochannel for wetting based sensing, *Nat. Commun.* **11**, 814 (2020).
- [84] D. Lohse, Fundamental fluid dynamics challenges in inkjet printing, *Annu. Rev. Fluid Mech.* **54**, 349 (2022).
- [85] B. Pan, M. O. Valappil, R. Rateick, C. R. Clarkson, X. Tong, C. Debuhr, A. Ghanizadeh, and V. I. Birss, Hydrophobic nanoporous carbon scaffolds reveal the origin of polarity-dependent electrocapillary imbibition, *Chem. Sci.* **14**, 1372 (2023).
- [86] P. Dwivedi, D. Pillai, and R. Mangal, Self-propelled swimming droplets, *Curr. Opin. Colloid Interface Sci.* **61**, 101614 (2022).
- [87] D. Lohse and X. Zhang, Physicochemical hydrodynamics of droplets out of equilibrium, *Nat. Rev. Phys.* **2**, 426 (2020).
- [88] M. Rashidi, M. Zargartalebi, and A. M. Benneker, Mechanistic studies of droplet electrophoresis: A review, *Electrophoresis* **42**, 869 (2021).
- [89] S. Yu, Y. Jing, Y. Fan, L. Xiong, H. Wang, J. Lei, Y. Zhang, J. Liu, S. Wang, X. Chen, H. Sun, and X. Hou, Ultrahigh efficient emulsification with drag-reducing liquid gating interfacial behavior, *Proc. Natl. Acad. Sci. USA* **119**, e2206462119 (2022).
- [90] V. Levich and V. Krylov, Surface-tension-driven phenomena, *Annu. Rev. Fluid Mech.* **1**, 293 (1969).
- [91] A. C. Payatakes, Dynamics of oil ganglia during immiscible displacement in water-wet porous media, *Annu. Rev. Fluid Mech.* **14**, 365 (1982).
- [92] S. An, Y. Zhan, H. Mahani, and V. Niasar, Kinetics of wettability alteration and droplet detachment from a solid surface by low-salinity: A lattice-Boltzmann method, *Fuel* **329**, 125294 (2022).
- [93] W. Lei, X. Lu, T. Wu, H. Yang, and M. Wang, High-performance displacement by microgel-in-oil suspension in heterogeneous porous media: Microscale visualization and quantification, *J. Colloid Interface Sci.* **627**, 848 (2022).
- [94] T. T. Al-Housseiny, I. C. Christov, and H. A. Stone, Two-phase fluid displacement and interfacial instabilities under elastic membranes, *Phys. Rev. Lett.* **111**, 034502 (2013).
- [95] B. Zhao, C. W. MacMinn, B. K. Primkulov, Y. Chen, A. J. Valocchi, J. Zhao, Q. Kang, K. Bruning, J. E. McClure, C. T. Miller, A. Fakhari, D. Bolster, T. Hiller, M. Brinkmann, L. Cueto-Felgueroso, D. A. Cogswell, R. Verma, M. Prodanović, J. Maes, S. Geiger *et al.*, Comprehensive comparison of pore-scale models for multiphase flow in porous media, *Proc. Natl. Acad. Sci. USA* **116**, 13799 (2019).
- [96] W. Lei, X. Lu, and M. Wang, Multiphase displacement manipulated by micro/nanoparticle suspensions in porous media via microfluidic experiments: From interface science to multiphase flow patterns, *Adv. Colloid Interface Sci.* **311**, 102826 (2023).
- [97] J. L. Anderson, Colloid transport by interfacial forces, *Annu. Rev. Fluid Mech.* **21**, 61 (1989).
- [98] C. C. Maass, C. Krüger, S. Herminghaus, and C. Bahr, Swimming droplets, *Annu. Rev. Condens. Matter Phys.* **7**, 171 (2016).
- [99] J. L. Moran and J. D. Posner, Phoretic self-propulsion, *Annu. Rev. Fluid Mech.* **49**, 511 (2017).
- [100] S. Michelin, Self-propulsion of chemically active droplets, *Annu. Rev. Fluid Mech.* **55**, 77 (2023).
- [101] A. Revil, A. Finizola, and M. Gresse, Self-potential as a tool to assess groundwater flow in hydrothermal systems: A review, *J. Volcanol. Geotherm. Res.* **437**, 107788 (2023).
- [102] V. S. Markin and A. G. Volkov, The phase boundary potentials at the interface between two immiscible electrolyte solutions, *Russ. Chem. Rev.* **57**, 1124 (1988).
- [103] J. Lützenkirchen, T. Preočanin, and N. Kallay, A macroscopic water structure based model for describing charging phenomena at inert hydrophobic surfaces in aqueous electrolyte solutions, *Phys. Chem. Chem. Phys.* **10**, 4946 (2008).
- [104] E. Chibowski and A. Wiacek, Electrokinetics of *n*-alkane oil-in-water emulsions, in *Interfacial Electrokinetics and Electrophoresis* (CRC Press, 2001), pp. 913–952.

- [105] J. H. Masliyah and S. Bhattacharjee, *Electrokinetic and Colloid Transport Phenomena* (John Wiley & Sons, Inc., New Jersey, 2006).
- [106] J. N. Israelachvili, *Intermolecular and Surface Forces*, 3rd ed. (Academic Press, San Diego, CA, 2011).
- [107] Y. Marcus, Thermodynamics of solvation of ions. Part 6.—The standard partial molar volumes of aqueous ions at 298.15 K, *J. Chem. Soc., Faraday Trans.* **89**, 713 (1993).
- [108] T. Wandlowski, V. Marecek, K. Holub, and Z. Samec, Ion transfer across liquid-liquid phase boundaries: Electrochemical kinetics by Faradaic impedance, *J. Phys. Chem.* **93**, 8204 (1989).
- [109] Y. Marcus, M. Kamlet, and R. Taft, Linear solvation energy relationships: Standard molar Gibbs free energies and enthalpies of transfer of ions from water into nonaqueous solvents, *J. Phys. Chem.* **92**, 3613 (1988).
- [110] E. Lac and J. D. Sherwood, Streaming potential generated by a drop moving along the centreline of a capillary, *J. Fluid Mech.* **640**, 55 (2009).
- [111] J. Sherwood and E. Lac, Streaming potential generated by two-phase flow in a polygonal capillary, *J. Colloid Interface Sci.* **349**, 417 (2010).
- [112] J. D. Sherwood, Y. Xie, A. van den Berg, and J. C. T. Eijkel, Theoretical aspects of electrical power generation from two-phase flow streaming potentials, *Microfluid. Nanofluid.* **15**, 347 (2013).